Development of Wire Mesh Type Probe for Void Measurement

M. Tech

Project Report

Submitted in fulfillment of the requirement for the degree of Master of Technology

By

Mahendra Prasad
Roll No: 99317301

Under the guidance of

Prof. Kannan N. Iyer

And

Prof. P.C. Pandey

Energy Systems Engineering
Indian Institute of Technology, Bombay
January, 2001

Dissertation Approval Sheet

This is to certify that the dissertation titled "***Development of Wire Mesh Type Probe for Void Measurement*** ", submitted by Mahendra Prasad, Roll Number: 99317301 has been approved for the degree of *Master of Technology in Energy Systems Engineering.*

Signature of Guide

Signature of Internal Examiner

Signature of Co-Guide

Signature of External Examiner

Signature of Chairman

Date: 15/1/01

ABSTRACT

The knowledge of void fraction (fraction by volume of gas phase to a total given volume) forms an important part of two-phase analysis. This kind of flow occurs widely in industries, in a number of forms that depend upon the prevailing conditions. A number of techniques have been developed and tested by different researchers so far. The complexity of two-phase flow has made it difficult to develop a universal void measuring system. The present work attempts to develop a wire mesh probe, which should overcome some of the problems associated with void measurement. Chapters, 1 and 2 present a detailed literature survey on void fraction measurement techniques. In the third chapter, the electronic circuit development for the wire mesh probe is described. Finally, measurements detail using the probe is outlined.

CONTENTS

LIST OF FIGURES

LIST OF TABLES

LIST OF SYMBOLS AND ABBREVIATIONS

Symbol	Designation
C:	Capacitance
D_E:	Distance of Separation of Electrodes
E:	Electric Field
e:	Charge Density of Electrodes
G:	Conductance
G_E*:	Dimensionless Conductance
H:	Liquid Hold-Up
h_L:	Thickness of Liquid Film
R:	Resistance
V:	Electric Potential
Z:	Impedance
α :	Void Fraction
$\in$:	Dielectric Constant
γ :	Conductivity
ρ_w:	Density of Water
ρ_a:	Density of Air

Abbreviation	Explanation
A.C.	Alternating Current
D.C.	Direct Current

ADC	Analog-to-Digital Converter
CRO	Cathode Ray Oscilloscope
D.P.T.	Differential Pressure Transducer
Opamp	Operational Amplifier

Chapter 1
INTRODUCTION

The simultaneous flow of gas and liquid in an enclosed duct is termed as two-phase flow. If the gas and liquid are the two phases of a single fluid then the flow can be termed as two-phase flow of single component fluid or, simply, two-phase flow (e.g. water–steam flow). Sometimes the two phases of the flow are of different fluids (e.g. air-water flow, natural gas-crude oil flow). Generally, the lower density fluid (the gaseous phase) is used to define the term void fraction. It is defined as the ratio of the gas phase in a given volume of the pipe or duct to the total volume.

$$\alpha_V = \frac{V_g}{V}$$

Alternatively, it can be defined as the fraction of the total cross-sectional area, A, occupied by the gas phase averaged over time.

$$\overline{\alpha}_A = \frac{\int_{t_1}^{t_2} A_g(t)dt}{A(t_1 - t_2)}$$

The void fraction can then be written as $\alpha = \overline{\alpha}_A = \alpha_V$.

1.1 Significance of Void Fraction Measurement

Two-phase flow is found widely in industries such as thermal and nuclear power plants, oil-water pipelines, refrigerating and condensing plants, etc. The two-phase flow occurs in a variety of patterns in horizontal and vertical ducts. The pattern of flow is dependent upon a large number of factors like temperature, pressure, flow velocity, inside surface of the duct, etc. The most general, and common classification for a horizontal pipe is depicted in Fig. 1.1. In a vertical pipe all the

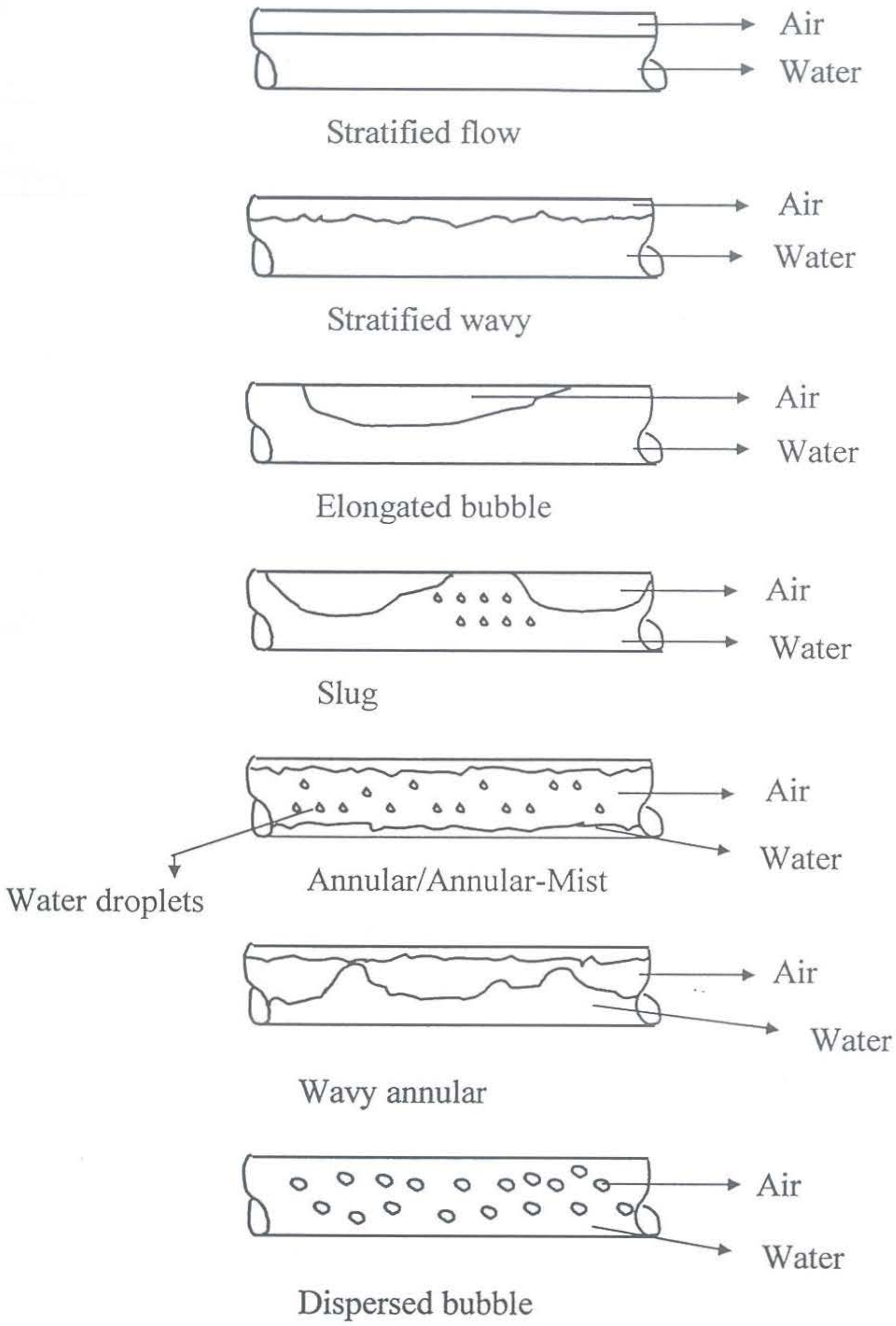

Fig. 1.1. Different types of two-phase flow
in an horizontal pipe

types of flows that are shown in the figure occur, except the stratified flow .The mass, momentum, and heat transfer equations are strongly dependent upon the type of flow and the void fraction.

1.2 Measurement Techniques

Void fraction measurement techniques can be classified into four main types:

a) Channel averaged measurement
b) Chordal averaged measurement
c) Local void measurement
d) Cross-sectional averaged measurement

a) Channel averaged measurement : This type refers to the measurement of void fraction over a full section (volume) and averaged over it. Quick-closing valves are involved in the measurement of void fraction. The advantage of using such a valve is the ease in measurement. Since the closing of the valves takes finite amount of time, this introduces certain inaccuracy in the measurement.

b) Chordal averaged measurement : This method measures average void fraction across a chord of the channel. Beam of X-rays or γ-rays is passed in the channel and these get attenuated, depending on the relative quantities of liquid and gas, by a combination of photo-electric, pair production, and Crompton Scattering effects. This method is much faster, and accurate than the earlier one. There are few problems associated with this method like safe handling of radiation, statistical errors due to random nature of creation of photons, and orientation of void and its fluctuation with time. Also, this method is relatively more costly.

c) Local void measurement : This is a time-averaged measurement at the chosen position. Electrical probes are normally used for this purpose. The advantages of using electrical probes are their simplicity in fabrication, relatively lower cost of the components, and fast response.

d) Cross-sectional averaged measurement : Neutron scattering method is utilized for cross-sectional average measurements. A neutron beam is passed through the test section and the scattered, and transmitted fluxes are measured by counting. The problems associated with this method are the availability of the neutron source, and the cost of instrument.

1.3 Types of Sensors

Depending upon the physical properties of the two-phases in a two-phase flow, there are a number of sensors that are used in various types of measurements. Various types of probes/sensors are as following:

a) Optical probes : When the two phases have different refractive indices, this types of probe is used to detect the void fraction at a chosen point. The time of presence of a phase at a point can be measured to calculate local time average void fraction.

b) Radiation sensors : These sensors exploit the phenomenon of radiation attenuation. When the two phases have different attenuation coefficients, void fraction can be measured by comparing the radiation intensity before and after passing through the two-phases mixture. This is related to the void fraction through the attenuation coefficients.

c) Thermo sensors : If there exists a temperature difference between the two phases, void fraction can be determined by measuring the local phase temperatures with the help of micro-thermocouples.

d) Anemometric sensors : When the heat transfer coefficients of two phases are substantially different from one another then, hot wire or hot film anemometers can be used to detect the local void fraction.

e) Electrical probes : These probes work on the basis of difference in electrical properties possessed by the two phases. Depending upon the conductivity/permitivity of the two individual phases electrical probes are further classified into two categories. They may be either conductance type, or capacitance type.

Conductance probes : When the difference between the conductivity of two phases is substantially large, conductance probes are employed for measurement of void fraction. The conductivity of a two-phase mixture depends upon the individual contribution of each phase. This is related to the void fraction.

Capacitance probes : When the relative permitivity i.e. dielectric constants of two phases are different, relative amount of the phases determines the resultant capacitance that is related to the void fraction. Dielectric constant depends upon the temperature of a substance and the frequency used to excite this substance. Use of capacitance probes is based on the fact that the dielectric constant of solid or liquid is very large as compared to the dielectric constant of the gaseous phase.

1.4 Project Objective

The objective of the project was to develop a void measuring probe. The features that needed to be incorporated were precision in void measurement, simplicity in fabrication of the mechanical system, ease in operation, and relatively low overall cost. The electrical probes offer these advantages.

1.5 Report Outline

The report is spread over five chapters. The first chapter introduces the basic definition of void fraction and its importance in some of the industries. Few measurement techniques and probe types are also described. In the second chapter, a detailed literature survey of some of the probes based on conduction, and capacitance principle is described. The third chapter describes the development of the electronic circuit for a wire mesh type of probe. The fourth chapter discusses the experiment carried out to measure void fraction by the wire mesh type probe. The last chapter gives the conclusion, and discusses some of the problems associated with the probe system that was used in the experiment.

Chapter 2

TYPES OF ELECTRICAL PROBES

In the previous chapter, a brief outline of the various techniques to measure void fraction, and various probes/sensors was described. Among all the probes/sensors used, electrical probes are the most popular due to the relative simplicity in fabricating them, their fast response, and relatively low cost of instrumentation.

2.1 Principle of Conductance Measurement

When a potential is applied between the electrodes, in an electrolyte, there is movement of ions of the electrolyte towards the electrodes. The flow of current depends upon the effective conductivity of the medium. In a two-phase condition, any change in the relative amounts of the two-phases is reflected in the measurement of current, or voltage since the effective conductivity of the two-phase depends upon the void fraction. Thus, the void fraction is known by measuring the change in voltage output when the system has only one phase, say water, and when it has two-phase mixture of water, and a gas. To eliminate the effects of polarization and capacitance, the frequency of the system is chosen suitably. Based on the geometry of the probe electrode, conductance probes are classified into-

a) Point type probe
b) Parallel plate type probe
c) Ring type probe
d) Sector type probe

The conductance probes are described in the following four sections. Subsequently some capacitance type probes will be described. A wire mesh type probe is described in the last section. The wire mesh type probe offers a novel way to measure void fraction because the results obtained are independent of the types of flows.

2.2 Point Type Probe

The principle of two-phase flow measurements by conductance probe is based upon the difference in the conductivity between the gas and liquid phase. In an air-water mixture, air can be considered as electrically insulating since its conductivity is around 10,000 times smaller than that of water. When the sensor is in contact with the liquid medium, the circuit gets closed and it opens up as soon as the sensor tip is in contact with air. The probe acts like a switch, the on and off time being a representative of the amount of liquid and gas at the point of measurement. While liquid contact gives instant response, gas contact does not give as fast a response due to finite de-wetting time.

The probe design proposed by Zwahr [1] is shown in Fig. 2.1. It consisted of a platinum wire of about 30 μm diameter, insulated by glass except at the front end. The tip of the probe had to be sharp enough to achieve immediate piercing with little deformation of the bubble at the moment of contact. This type of probe geometry also helped in the rapid de-wetting of the tip. The two sensors in the probe have a common stainless steel sheath which serves to maintain a well-defined sensor distance and easy handling of the probe.

Based on experimental investigations, it was concluded that the distance between the tips should be less than 20 mm to avoid loss of correlation between the signals due to turbulence. The most suitable distance between the tip for accurate determination of time delay was found to be 10 mm. The analog signal obtained from the probe was conditioned. Necessary care was taken so that all the information in the original signal was converted into a form suitable for

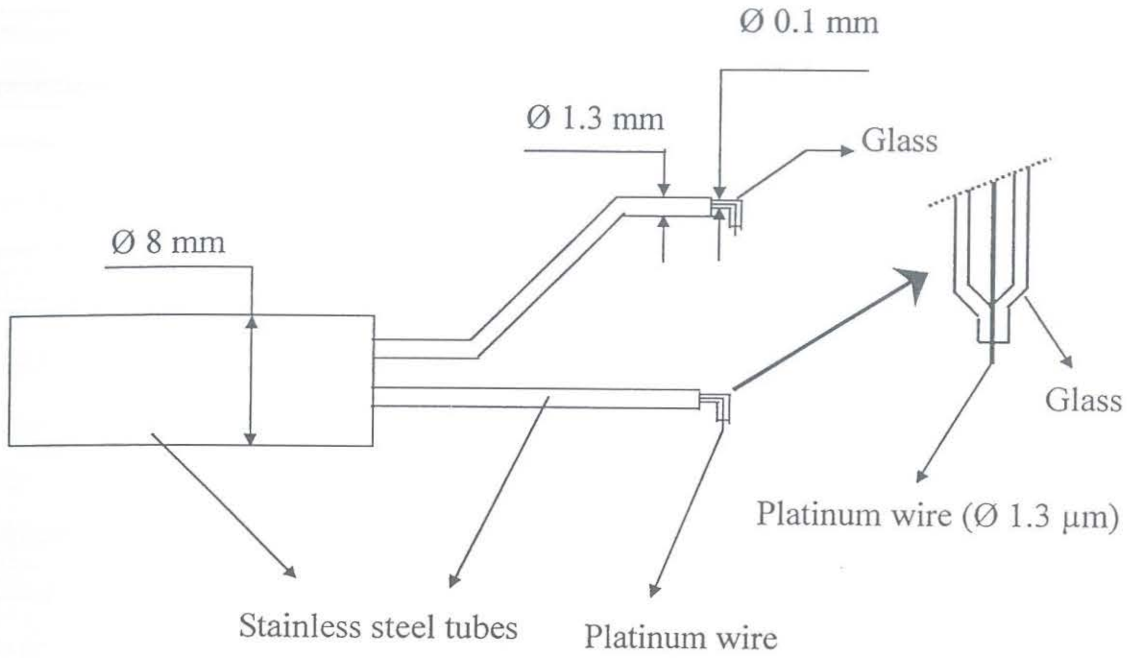

Fig. 2.1. Probe geometry for point type probe [1]

subsequent handling by the digital microprocessor that performed signal processing.

To achieve desired reliability, and accuracy in conditioning the signal, a signal trigger level was selected which was close to the output signal to minimize the effect of de-wetting time, and to take into account the presence of small bubbles. However, the trigger level was still on the wrong side when high void fractions were measured. Welle [2] avoided this disadvantage by first sampling the signal by an A/D converter and then comparing the samples with two self-adjusting trigger levels. Fig. 2.2 shows the block schematic, and condition table for this method. All the arithmetic operations were carried out using TTL hardware driven by clock of A/D converter. This is done so as to match the high conversion speed of A/D converter, which was about 250 kHz. Arithmetic operations were executed within the conversion time of the A/D converter, there by permitting simultaneous processing. Further processing of the resulting square wave signal consisted of sampling the square wave at a frequency, adjustable between 1, and 16 kHz, whose order was prescribed by the capability of the processing unit. The final sampling resulted in a number of zeros and ones representing the square wave in digital a form.

The local void fraction was measured by lower probe tip. It was defined as a time average of the concentration "c" by

$$\alpha = \lim_{T \to \infty} \frac{1}{T} \int_0^T c(x,t)\, dt \qquad 2.1$$

where, "c" is a function of place "x" and time "t". The concentration "c" was one, if the probe tip was in gas phase, and zero if the probe tip was in the liquid phase. As the signal was given in discrete form the above equation can be written as,

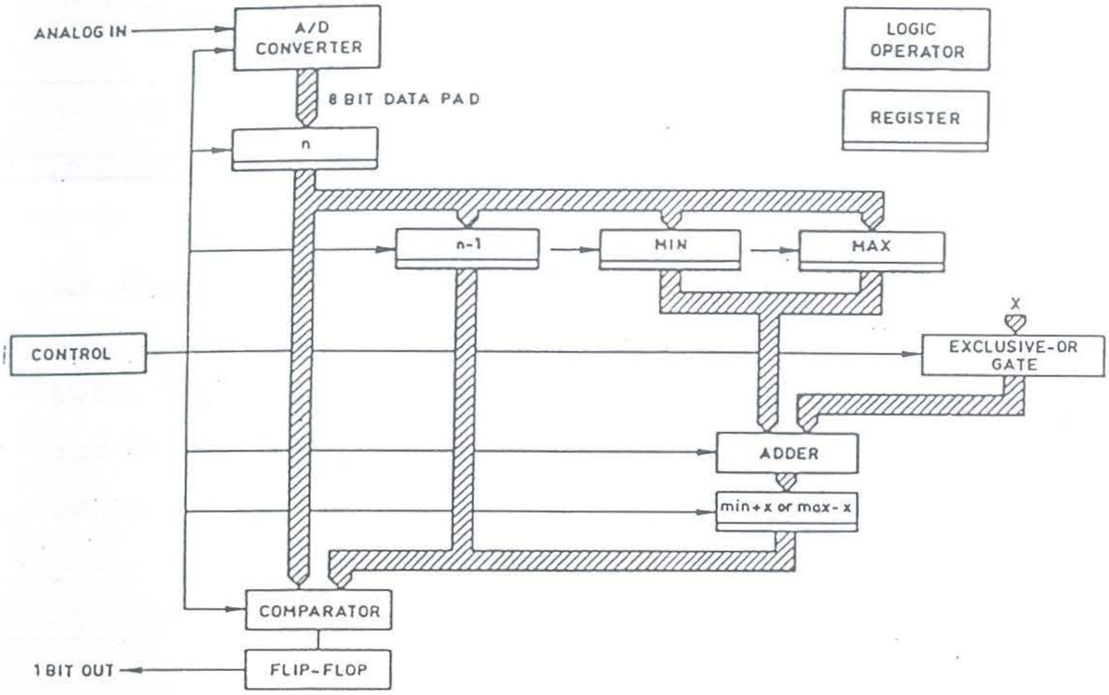

condition	minimum	maximum	output
n > n - 1	q	n	q
n = n - 1	q	q	q
n < n - 1	n	q	q
n > min + x	n	n	1 ↑
n < max - x	n	n	0 ↓

q = no change

Fig. 2.2. Block diagram and condition table [2]

$$\alpha = \frac{1}{T}\sum_{i=1}^{N} a(i) \qquad 2.2$$

where, N = Total number of samples

$\alpha(i)$ = Number of samples indicating presence of gas phase at the probe tip

The void fraction measurements were checked by comparing with void fraction obtained by the gamma photon technique. The result is shown in Fig. 2.3.

2.3 Parallel Plate Type Probe

Meftah [3] employed conductance method to measure void faction, where in he used an array of sensors to provide rapid indication of spatial, and temporal changes in void fraction.

An array of conductivity sensors was developed for a Scaled Model Boiling Water Reactor (SMBWR) as shown in Fig. 2.4. It consisted of a boiling water channel, steam separator manual control value, condenser, and fuel water pump. The channel was made up of 7740 Pyrex glass with an outside diameter of 50 mm, inside diameter of 46 mm, and length 508 mm.

The conduction probe sensor consisted of two parallel stainless steel plates 20 mm in length, and 10 mm in width, that were separated by a distance of 20 mm as shown in Fig. 2.5, and Fig. 2.6. There were five probes positioned at fixed axial positions. The distance between two adjacent probes was 76.2 mm as is shown in Fig. 2.7. The lowest probe (reference probe) was always placed in the liquid phase.

Meftah [3] had used manometer technique to relate the void fraction to the conductivity. In Fig. 2.8 an air-water test loop for the manometer measurement is shown. The height difference was proportional to the void fraction.

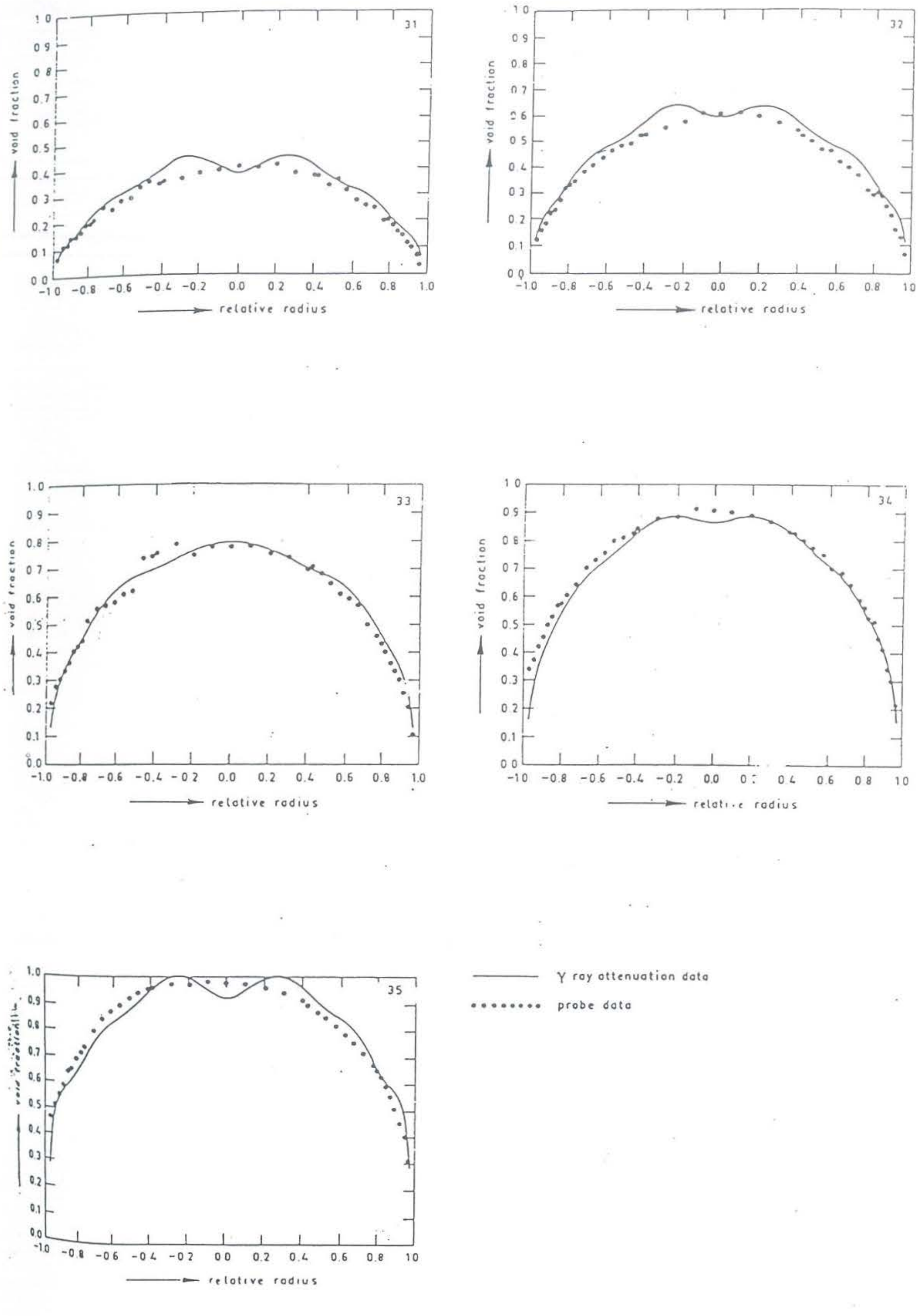

Fig. 2.3. Radial distribution of void fraction obtained by gamma photon technique, and point type probe [2]

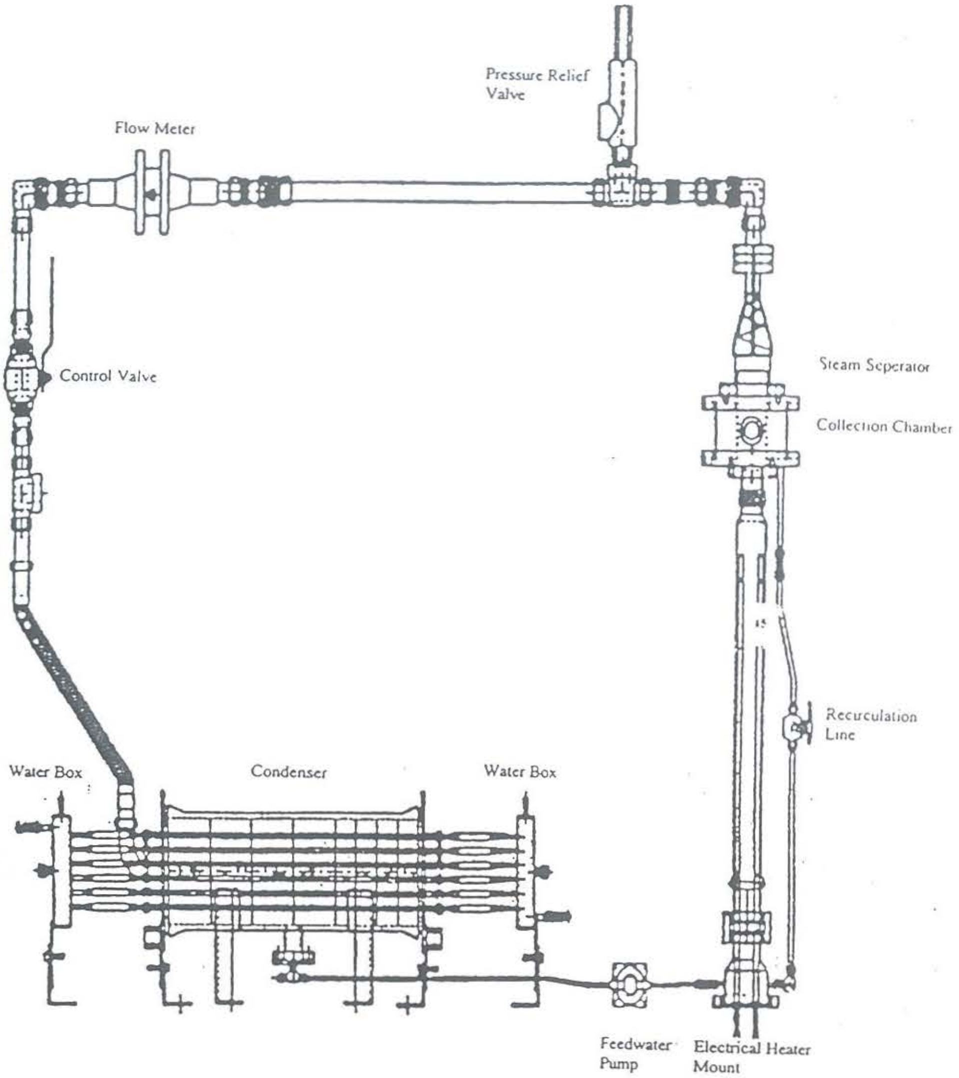

Fig. 2.4. General schematic of a SMBWR [3]

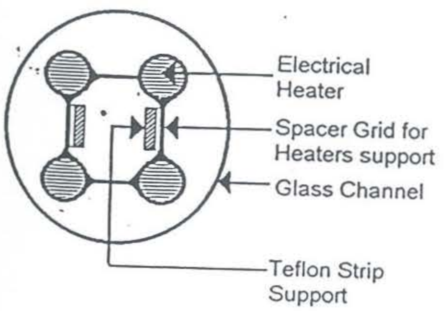

Fig. 2.5. Top view of boiling water channel [3]

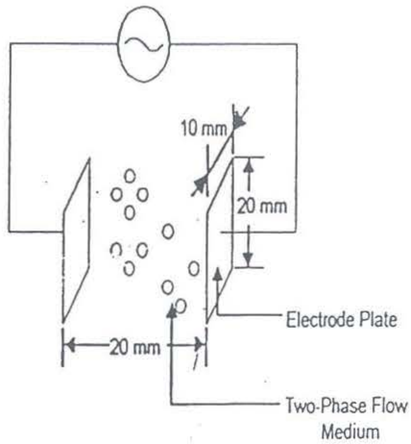

Fig. 2.6. A single electrode pair [3]

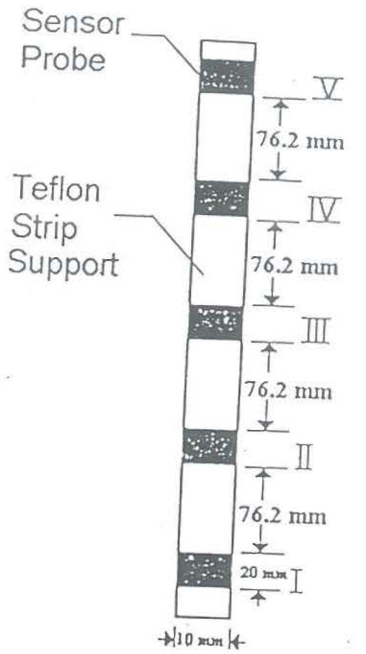

Fig. 2.7. Axial location of the parallel plate type probes [3]

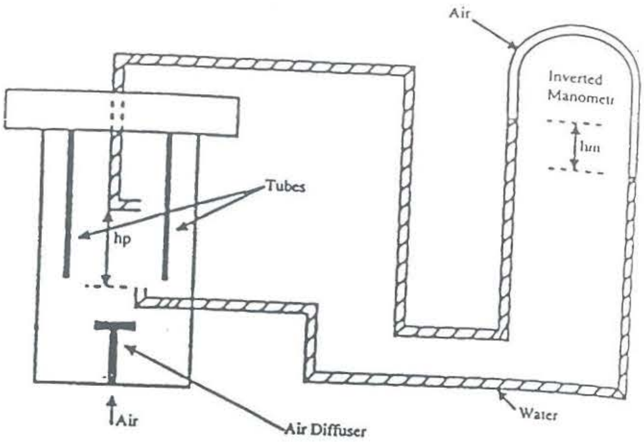

Fig. 2.8. Air water test loop [3]

When bubbles passed by the electrode plates, the conductivity of the medium between the plates was lowered since air-conductivity is much less as compared to the conductivity of water. The output voltage was proportional to the conductivity of the medium. A time average of 30 seconds was used in this process. The ratio, of the voltage output when two-phase mixture was present to the voltage output when only liquid phase was present, was compared with the manometer reading. A time averaged voltage ratio was plotted against void fraction as shown in Fig. 2.9 and compared with the Maxwell's theoretical curve. As can be observed, the two match each other up to the void fraction value of 20 percent, while for larger values the deviation is significant This is because at large void fractions the flow is no longer bubbly but deviates to slug type flow.

2.4 Ring Type Probe

A ring type probe has two annulus ring electrodes that are mounted in flush to the pipe wall. These rings are energized with a suitable voltage, and frequency to measure only the conductance across the two electrodes. The conductance depends upon the distance between the electrodes, and the liquid height.

When an appropriate high frequency signal was used, the effect of capacitance was very small as compared to that of the resistance. The conductance (inverse of resistance) is given, by,

$$G = \frac{\gamma}{\in}.C \qquad 2.3$$

where,

C = capacitance
$\in$ = dielectric constant of liquid
γ = conductivity of liquid

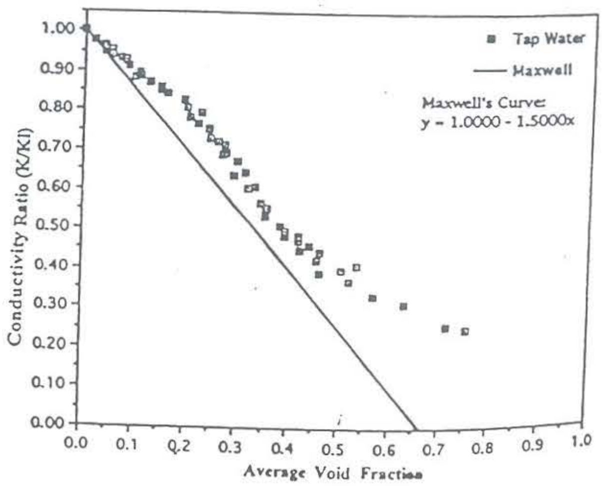

Fig. 2.9. Void fraction result using the parallel plate type probe [3]

Ring electrodes had been used by Andreussi [4] to predict liquid fractions in annular stratified, and bubbly flows. Tsochatzidis [5] had also used similar probe to measure liquid fraction in pipes under stratified flow conditions.

A schematic of the ring probe, used by Andreussi [4], is shown in Fig. 2.10. Following notations are used in this section,

L_E = πD = length of the ring
D_E = distance between electrodes
h_L = liquid film thickness ($h_L << D_E$)
e = charge density of electrodes

Assuming that the electric field, generated by charge density e, is contained within the tube, the magnitude and direction being constant, the potential drop between the two electrodes is given by,

$$\Delta V = \frac{e}{\in \pi D h_L} D_E \qquad 2.4$$

and capacitance by,

$$C = \frac{\in \pi D h_L}{D_E} \qquad 2.5$$

where, π D h_L = area of the liquid film.
The conductance, therefore, is given by

$$G_E = \frac{\gamma . \pi D h_L}{D_E} \qquad 2.6$$

It had also been shown by Asali [6], that the above equation was valid for $h_L << D_E$ and the frequency of A.C voltage greater than 100 kHz. At such a high frequency,

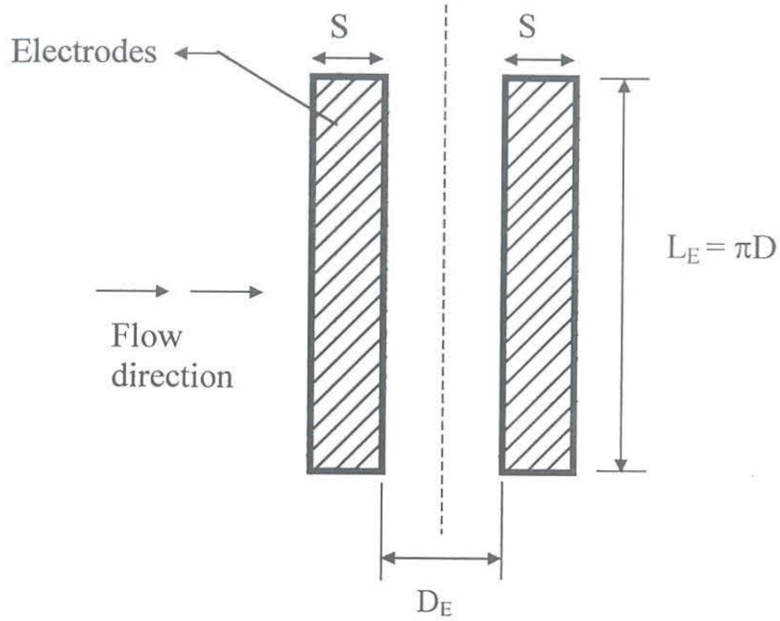

Fig. 2.10. Ring electrode [4]

the capacitive impedance was relatively much larger than resistive impedance. From above equation, one can observe that the conductance is proportional to flow area occupied by the liquid film.

A convenient experimental procedure to determine directly the liquid hold-up, H_L, without knowing the electrical conductivity of the liquid, consisted of the measurement of the ratio G_E^*, defined as the ratio between the conductance at a given hold-up, and conductance for the pipe for stratified, and annular flows. In Fig. 2.11 is shown the variation of the G_E^* with liquid hold-up for the annular, and stratified flows. From these figures it can seen that, for separation distances larger than two tube diameters, the calculated values of G_E^* were very close to the values of the liquid hold-up.

When the Maxwell's [7] equation for the equivalent conductivity of dispersed flow

$$\gamma = \frac{2H_L}{3-H_L}\gamma_L \qquad 2.7$$

and Bruggeman's [8] equation,

$$\gamma = H_L^{3/2}\gamma_L \qquad 2.8$$

where, γ is the equivalent conductivity, and γ_L is the conductivity of the liquid phase, was assumed to follow the actual values, then G_E^* was given by

$$G_E^* = \frac{2H_L}{3-H_L} \qquad \text{(Maxwell)} \qquad 2.9$$

and

$$G_E^* = H_L^{3/2} \qquad \text{(Bruggeman)} \qquad 2.10$$

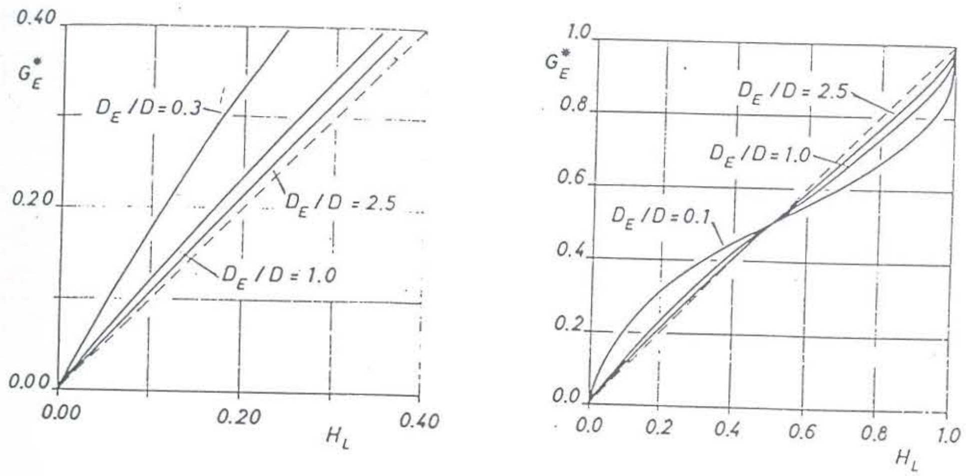

Fig. 2.11. Prediction for (a) Stratified flow, and (b) Annular flow at varying distances between the electrodes [4]

The plot of G_E^* vs. H_L is shown in Fig. 2.12.

Andreussi [4] had used three-ring probe structure where in the distance between the rings could be varied as shown in Fig. 2.13. He had used an excitation frequency of the order of 100 kHz. The electronic circuit, basically, consisted of an operational amplifier, and a low pass filter. The output signal from the amplifier was proportional to the liquid hold-up. From this signal, H_L was obtained as the ratio between the actual signal and the signal when only water flowed in the pipe.

The probes were calibrated for three types of flows. Inserting cylindrical glass rods of known diameter into the pipe simulated annular liquid films. Fig. 2.14a shows the result of such a simulation. It can be noted that for $H_L < 0.1$, G_E^* coincides with H_L. When the glass rods were placed off center, there were no appreciable affects on the conductance measurements.

Pouring known volumes of liquids into a short horizontal section of the pipe simulated stratified flow. The comparison between the theoretical, and the experimental results is shown in Fig. 2.14b. It is interesting to observe that, for both the annular and stratified flows, the experimental results tend to be closer to the line, at an angle of 45°, passing through the theoretical predictions. Bubbly flow conditions were simulated by a number of plastic spheres of known diameter (1-10 mm), suspended at fixed positions. Air, fed from the bottom, was also used to simulate bubbly flow. The comparison between the theoretical and experimental results for the bubbly flow is shown in Fig. 2.14c.

The ring type probe was proved effective for void fraction measurements, but it suffered, as all others, from a major limitation that this probe was very sensitive to the flow pattern transitions that are encountered widely in the two-phase flows. Next, we discuss a technique to measure void fraction that is independent of the type of flow pattern.

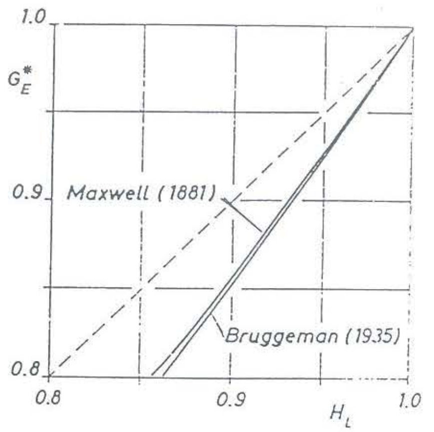

Fig. 2.12. Prediction for bubble flow [4]

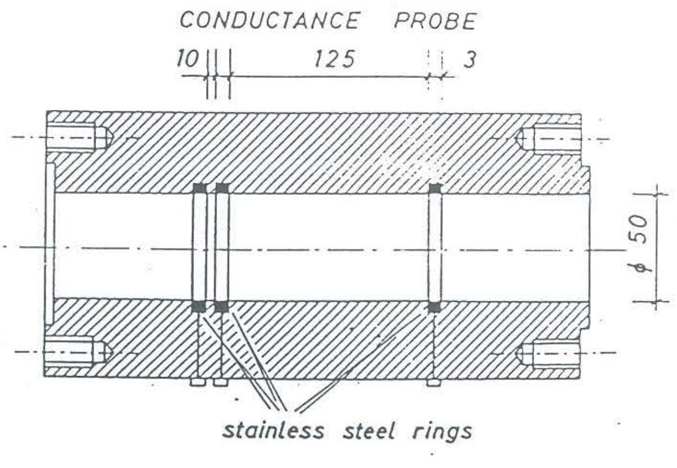

Fig. 2.13. Three ring probe structure [4]

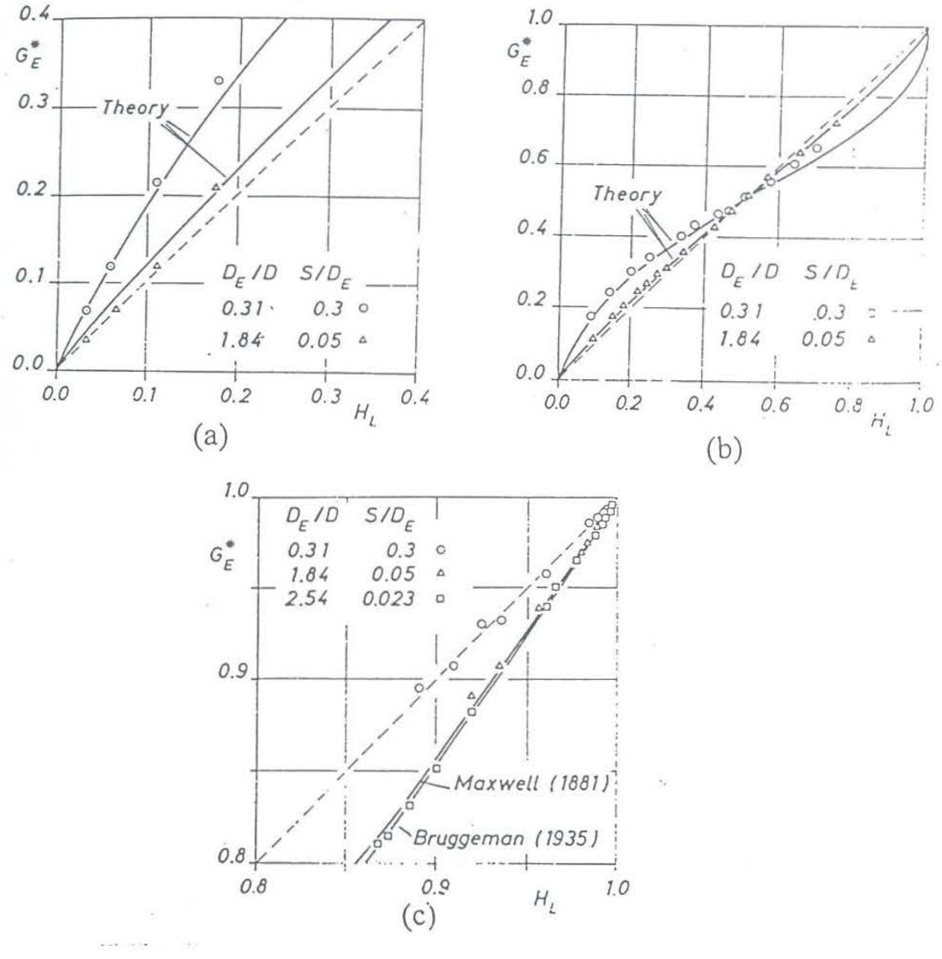

Fig. 2.14. Comparison between theory and experiment for
(c) Annular (b) Stratified (c) Bubble flow [4]

2.5 Sector Type Probe

The sector type of probe basically refers to the electrodes, in the form of cylindrical arc, which are put along the circumference, mounted in flush to avoid any obstruction to the flow.

Merilo, Dechene, and Cichowlas [9] had developed a sector type probe in which the electrodes formed a part of the tube wall, and the electric field, perpendicular to the flow, was rotated electronically to distribute it throughout the sensor.

The sector type probe consisted of six stainless steel electrodes, each of length 22.9 cm. A schematic view of this configuration is shown in Fig. 2.15. Ceramic insulators separated the electrodes from each other. The structure of the probe was like a polygon. The diameter of the test section was chosen to be 3.81cm.

A high frequency, 50 kHz, 10 V three-phase signal was used to excite the 3 electrode pairs. The phase difference between the excitations to two pair of electrodes was 120°. A rotating electric field, as is shown in Fig. 2.16, was produced .The absolute value of the signals from the three phases was summed up and the resultant was proportional to the average mixture conductivity between the sensors. To get relative conductivity of the two-phase with respect to the liquid phase, a reference sector probe was installed in a place where only single-phase (water) flowed, and the ratio of the output signal obtained from the reference sector probe to the output signal at the actual sector probe, where two-phase flowed, was related to the relative conductivity. A schematic diagram of the conductance measuring circuit is shown in Fig. 2.17.

Merilo [9] did conductance measurements on flowing air-water mixtures. The results of these measurements were compared with void fraction measurements, obtained by using quick closing valves. These valves were placed 57 cm upstream and downstream of the main sensor. The valves were driven by springs and

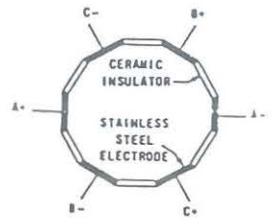

Fig. 2.15. Cross-sectional view of the sector type probe [9]

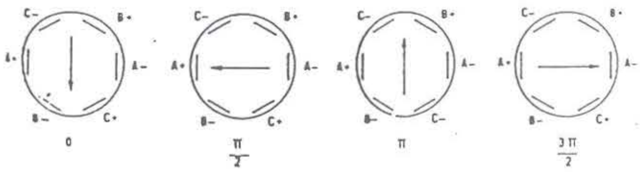

Fig. 2.16. Electric field vector in the middle of the probe [9]

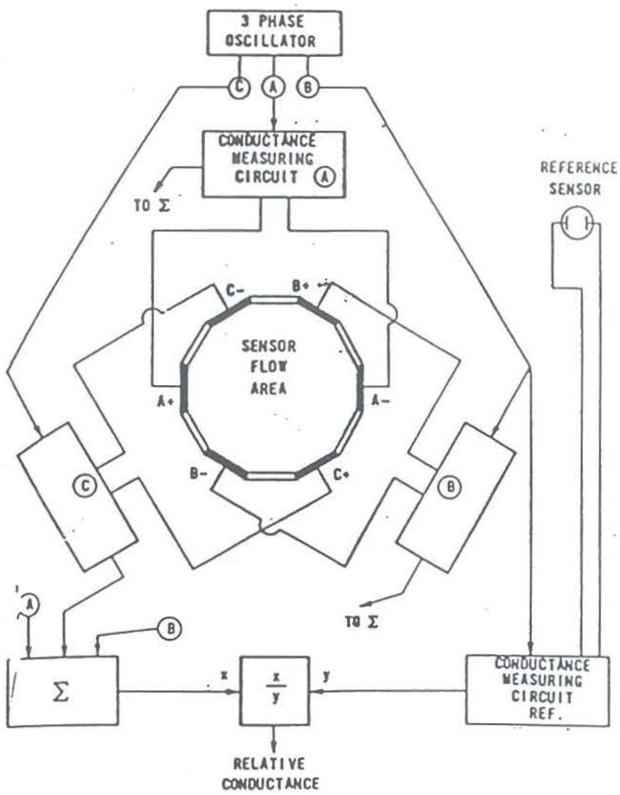

Fig. 2.17. Schematic diagram of conductance measuring circuit [9]

achieved a closure time of approximately 25 ms. The volume of water, that was trapped between the valves, was measured by draining it into a graduated cylinder. The water, and the air- flow rates were individually metered and controlled.

The experiments were conducted for both vertical up-flow, and horizontal flow. The gravitational effect caused asymmetry in air-water distribution in a horizontal flow. For the vertical up-flow, and the horizontal flow, the maximum superficial velocities of 2.5 m/s for water, and 60 m/s for air were used. The test section exit pressure varied from close to atmospheric pressure (at low flow rates) to 400 kPa (at higher flow rates).

In the experiment, the patterns were determined visually that had caused some error in measurements. Fig. 2.18 shows the variation of relative conductivity with void fraction, and compares the theoretical values with that predicted by Maxwell [7], and Bruggeman [8].

$$\frac{K_m}{K_0} = 1 - \frac{3\alpha}{2+\alpha} \qquad \text{(Maxwell)} \qquad 2.11$$

where, K_m was the mixture conductivity, and K_o was the continuous medium conductivity (liquid). This was derived for non- interacting equal size spheres of zero conductivity that were distributed in the continuous medium of conductivity K_o. This equation is valid for only low values of α..

$$\frac{K_m}{K_o} = (1-\alpha)^{3/2} \qquad \text{(Bruggeman)} \qquad 2.12$$

This equation was derived for random size spheres of zero conductivity. The spheres were randomly distributed throughout a continuous medium of conductivity K_o. K_m is the mixture conductivity. This equation is valid for any value of void fraction.

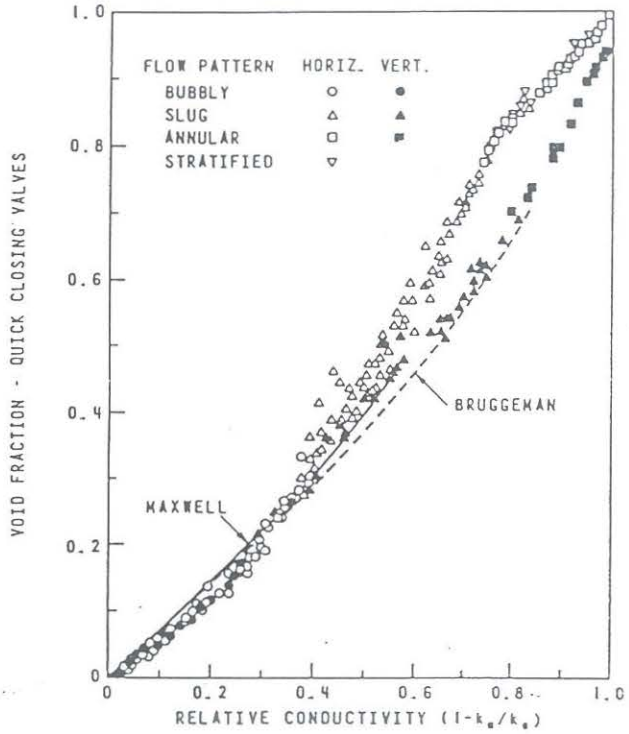

Fig. 2.18. Calibration curve for the sector type probe [9]

When the flow pattern was annular, the average conductivity of the two-phase mixture depended on the orientation of the test section. This was because the sector type probe essentially measured the film thickness of the liquid to which no conduction path was present. In a horizontal flow, the liquid film is highly asymmetric resulting in a lower conductance value than if the same amount of liquid were distributed uniformly.

In the slug flow regime, the difference between the vertical, and the horizontal orientations did not appear until the void fraction reached approximately 50 percent. These observations are consistent with the fact that slug flow is basically a combination of bubbly, and annular flows. In the low void fraction region of slug flow, the sensor sees predominantly bubbly flow for which the mixture conductivity is independent of orientation. As the void fraction increases, annular flow becomes predominant.

The sector type probe, using the rotating field concept, is a useful, and versatile way for void fraction measurements. But later on, the use of rotating field for void fraction measurement does not find mention, though sector probes using single-phase excitation, and certain modifications in the shape and size of the electrode, have been used.

2.6 Capacitive Probes

One of the important experiments in the field of void fraction measurement was done by Sami and Kendall [10], where they had used 5 different configurations. These are shown in Fig. 2.19. Though they had measured capacitance, those configurations could well be used for conductance probe development. Of all the six designs, designs number (d) and (f) gave best results. Fig. 2.20 gives another

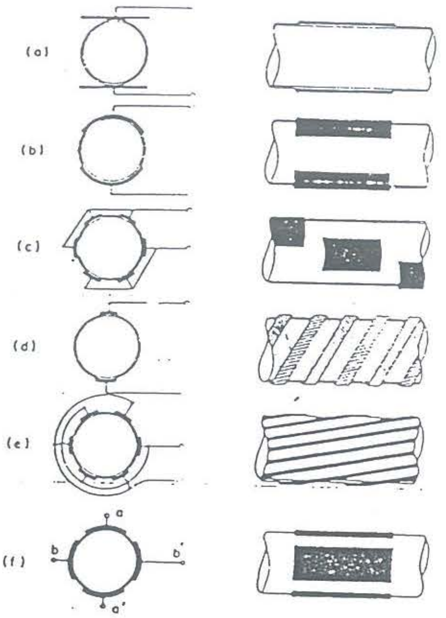

Fig. 2.19. Capacitor configurations (a) Parallel plates (b) Concave plates (c) Staggered concave plates (d) Double helix (e) Multiple helix (f) Four concave plates [10]

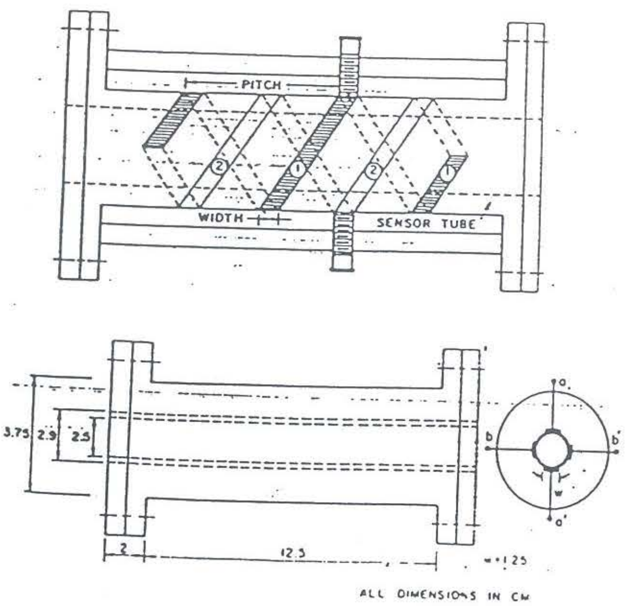

Fig. 2.20. Sensor structure for the configurations (d), and (f) [10]

view of the sensors (d), and (f). These sensors gave linear variation of the capacitance with void fraction. This is shown in Fig. 2.21, and Fig. 2.22.

Another capacitance measuring technique finds mention in a paper by Khalil, Mclutosh, and Boom [11]. Fig. 2.23 shows the probe configuration used by them. Similar type of work was also reported by Kendoush and Sarkis [12].

Jing Wang [13] had conducted experiments on two-phase flow of helium. This was different, from a water-air flow because the change in dielectric constant of helium from liquid to vapor phases is only 4%. This had necessitated the use of a sensitive capacitance circuit. The schematic of the half-cylindrical electrode sensor is shown in Fig. 2.24. It consisted of two 100 mm long, brassy, half-cylindrical electrodes separated by a Perspex support. In the set-up two guard electrodes and a double-layer shield for the whole capacitor was provided. The experiments were performed at 0.1 MPa, 20 °C environment Perspex work-ups. The results of the numerical simulation, and experiment are shown in Fig. 2.25.

2.7 Wire Mesh Type Probe

Kreper and Prasser [14] have reported a wire mesh probe to measure void fraction. The probe consisted of two sets of parallel wires with 16 wires in each set. The distance between two adjacent wires in one set was 3 mm. These two sets of parallel wires were pierced into a cylindrical tube (perpendicular to length) of diameter around 50 mm. The two set of parallel wires seemed to form two layers, and were separated by a distance of 1.5 mm. Fig. 2.26 shows the top view of the cylinder where the wires were pierced and these wires seem to form a grid. Thus, there were 256 points where the wires are seen to cross in the Fig. 2.26. For convenience the complete set-up, the mechanical system, and the electronic circuit, is shown in Fig. 2.27 where in only 4 wires in each set is shown. The electronic circuit consisted of 4 operational amplifiers, 4 Sample-and-Hold circuits, and 4

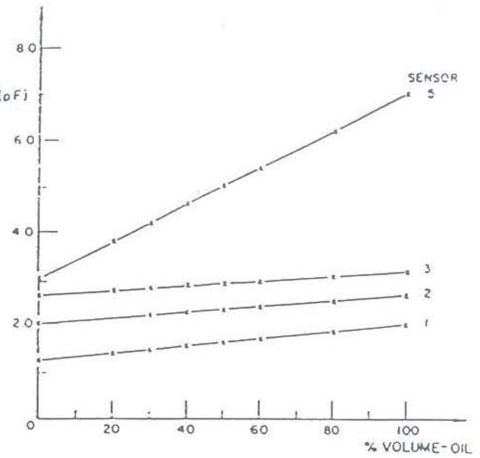

Fig. 2.21. Capacitance versus percentage volume-oil (type d) [10]

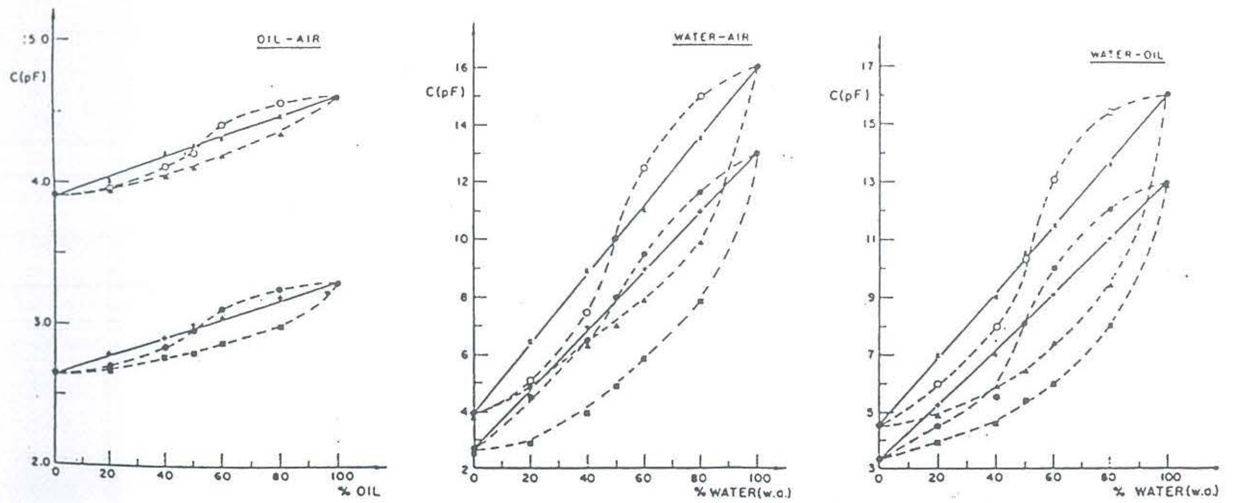

Fig. 2.22. Capacitance versus void fraction (type f) [10]

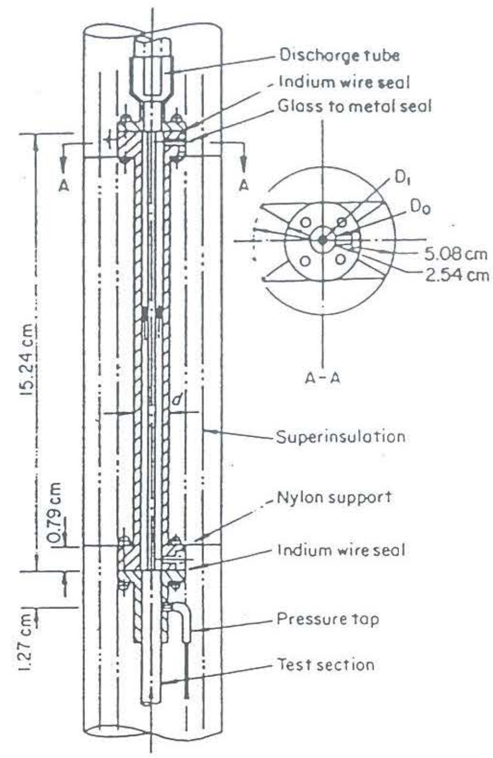

Fig. 2.23. Void fraction probe [12]

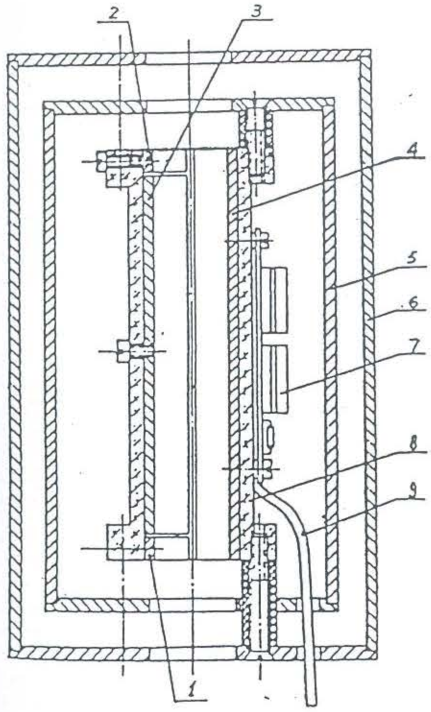

1,2 guard electrodes

3,4 electrodes

5 inner shield

6 external shield

7 Printed circuit boasd

8 Support

9 cable

Fig. 2.24. Half-cylindrical electrodes sensor [13]

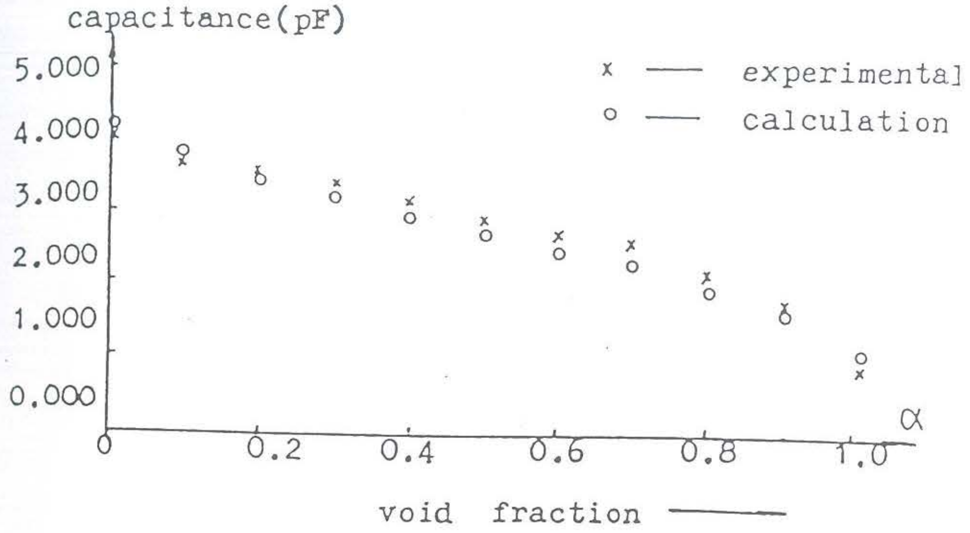

Fig. 2.25. Calibration, and calculation results [13]

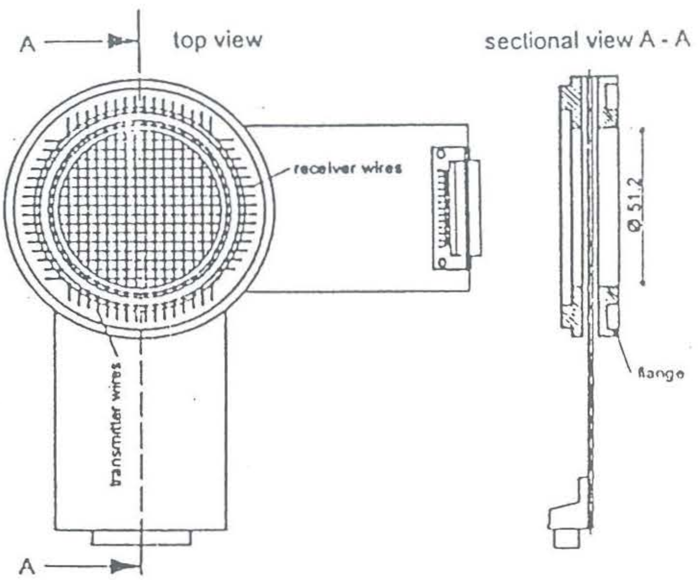

Fig. 2.26. Top view of the cylindrical tube [14]

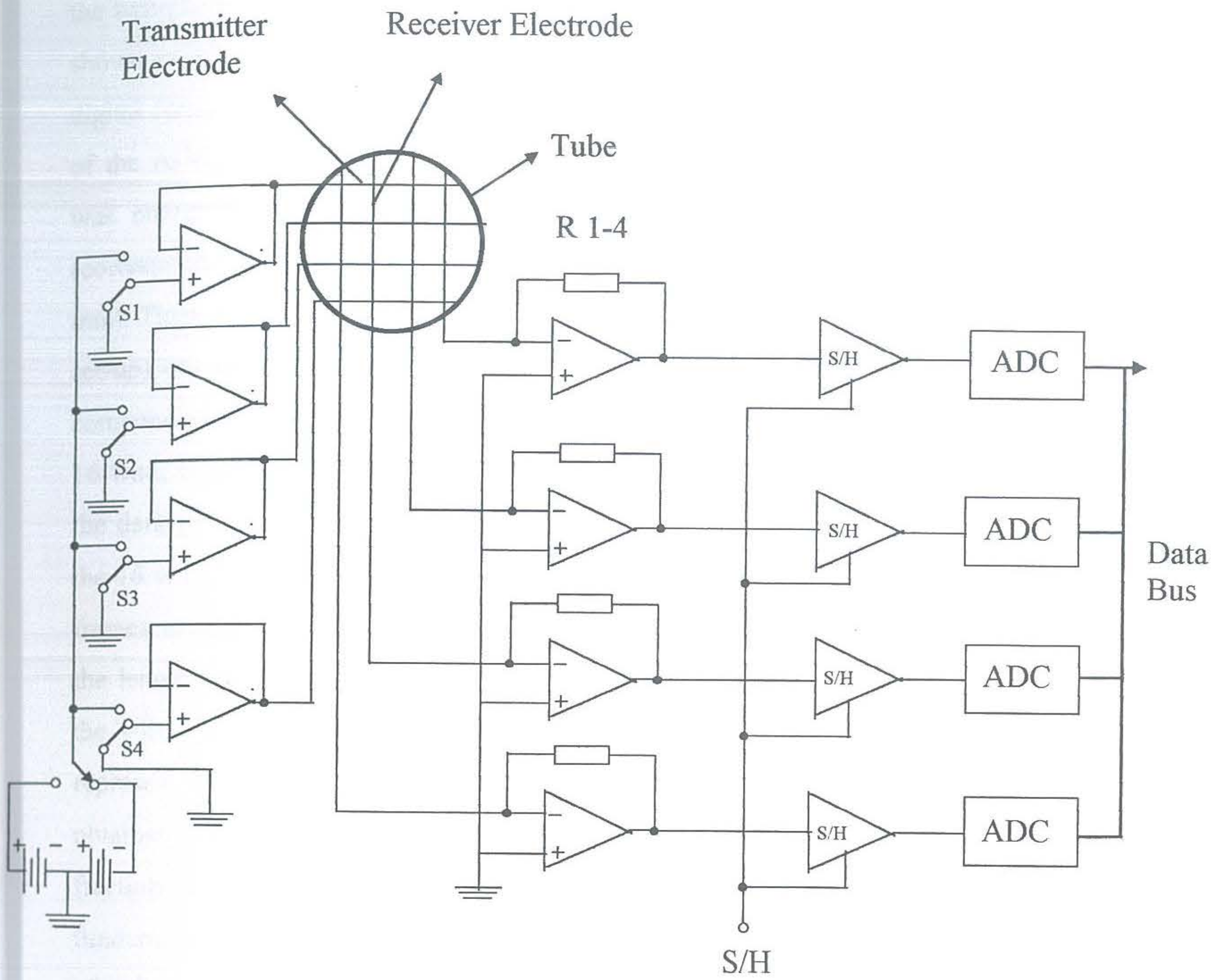

Fig. 2.27. Electronic circuit to measure void fraction [14]

ADC's. The principle of operation was to energize one wire in a set (transmitting wires in Fig.2.27) and pass the current, depending upon the impedance offered by the two-phase, to 4 I/V converters (operational amplifiers with feed back resistors shown as R1-4 in Fig. 2.27). The outputs of these converters were converted into digital form using the Sample-and-Hold circuits and the ADC's. The output lines of the ADC's were paralled and connected to a microprocessor. When one wire was energized 4 output voltages (or 16 in the actual set-up) were obtained (corresponding to the impedance offered by the two-phase in a distance of 1.5 mm). Then, other wires were energized and a total of 16 data (or 256 for the actual set-up) was obtained. These data were related to the spatial distribution of the two components of the two-phase flow. In Fig. 2.28, 256 data, obtained by energizing 16 wire, is shown as a frame where in the white portion shows the gas phase and the dark portion shows the water phase. By repeating the sequence of energizing the 16 wires more frames were obtained that are shown in the same figure. These frames were analyzed to pictorially represent the cross-section of a bubble (along the length) as shown in Fig. 2.28. The frames were utilized to get an estimate of the void fraction. The ratio of the lighter area to the darker area in a frame is representative of the void fraction. The sum of these ratios, for all the frames obtained over the time of experimentation, averaged over time would give the void fraction in the pipe. The probe used by Kreper and Prasser [14] employes a fundamental principle, yet simple, that a three-dimentional object is basically a set of infinite number of points, and to copy such an object is essentially to get the points and join them appropriately. The probe is very simple in construction, and the electronic circuit is also relatively easy to make. Inspired by this work an attempt was made to construct a similar kind of probe to measure void fraction. This is presented in the next two chapters.

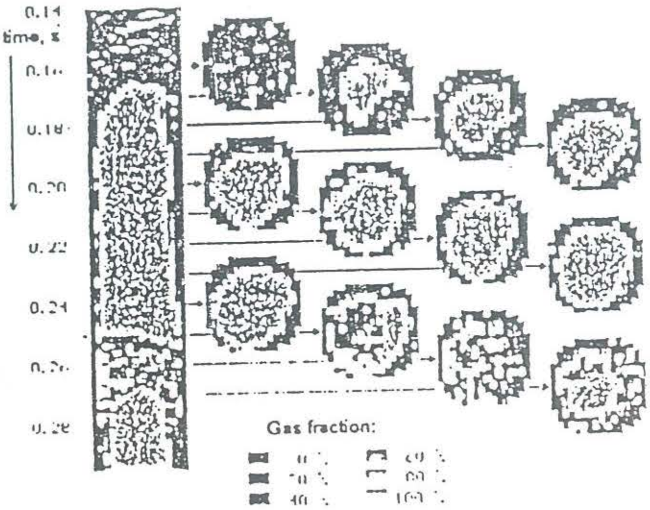

Fig. 2.28. Cross-sectional frames of the two-phase flow [14]

Chapter 3
VOID PROBE SYSTEM

In the previous chapter, a wire mesh type probe reported by Kreper and Prasser [14] has been described. The wire mesh probe offers one of the most promising ways to measure void fraction. This is primarily because the probe results are independent of the flow type. Additionally, the probe has fast response, relatively low cost of instrumentation, and can be used for various shapes of ducts like a coaxial pipe, etc. Use of other techniques of void measurement on shapes that are irregular or complicated is very difficult, but wire mesh type probe can be used comfortably in such situations. The project is based on such a probe system to measure void fraction in ducts.

3.1 Preliminary Investigation

In the wire mesh type probe, the current flowing between two electrodes, in response to an excitation voltage across the electrodes, is indicative of the impedance between the two electrodes. The sensed signal is converted using an ADC. The ADC used should have sufficient resolution to detect changes in the sensed signal. An experiment was carried out to find out the number of bits in the ADC to be used.

In this experiment, the electrodes were two stainless steel needles dipped in a glass container filled with water such that the needle tips were in contact with water. This is shown in Fig. 3.1. Sinusoidal excitation was given to one of the electrodes at one end through a voltage follower. The other electrode was connected to a current-to-voltage converter circuit. The current through the electrodes is given as,

$$I = V_s / Z \text{, where } Z = \text{impedance between the two electrodes}$$

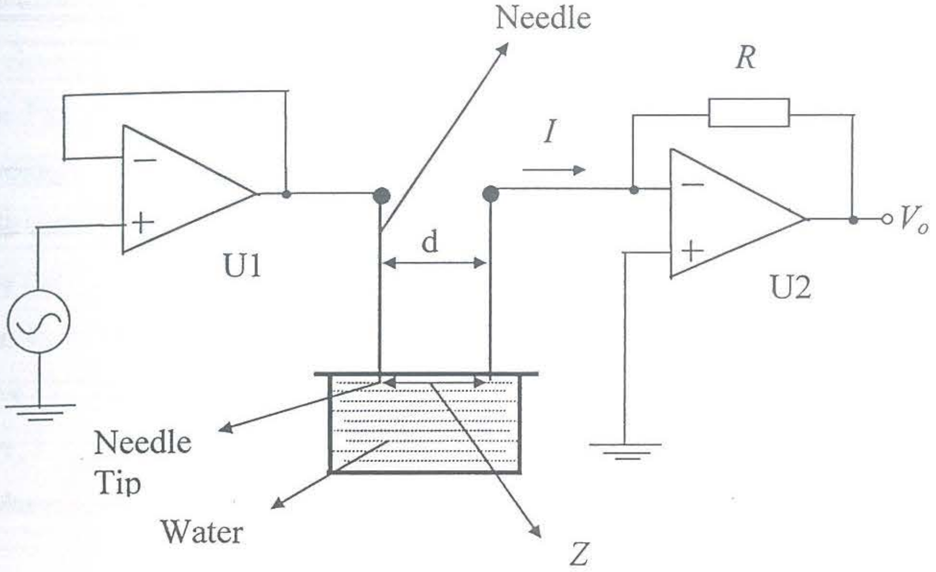

Fig. 3.1. Set-up for preliminary investigation
U1, U2: LF351
$R = 30$ k ohm

and the output voltage is given as,

$$V_o = -(R/Z)\ V_s$$

A plot of V_o vs. inter-electrode distance *d,* where *d* varied from 1 to 15 mm at approximately 1 mm interval by moving the needle, was obtained. It was difficult to place electrodes closer than 1 mm. The plot of V_o vs. inter-electrode distance *d* is shown in Fig. 3.2 for three different frequencies and the same value of V_s. The output voltage increases as the frequency increases. This shows that most of the current is capacitive. It can be observed from the plots that the output voltage decreases very sharply with the distance. The decrease is sharper as the frequency increases. In all the plots, the output voltage level at distances of 2, 3, and 4 mm are above 1/256 of the output voltage level at a distance of around 1 mm. Therefore, it was concluded that an 8-bit ADC would be needed to detect changes in the voltage level because of excitation distance in water.

3.2 Mechanical Assembly

For the purpose of the project, a cuboid block of size 30 mm x 30 mm x 30 mm was taken. The cuboid block was made of Perspex. In this block a hole of diameter 24 mm was drilled. Hypodermic needles, made of stainless steel (SS) of diameter 1 mm, were used to form two sets of parallel wires as shown in Fig. 3.3. The pitch (distance between two adjacent needles in each set of the parallel wires) was selected as 2 mm. The distance between the two sets of wires was also selected as 2 mm (Fig. 3.3). The pitch dimension selection was based on the work done by Kreper and Prasser [14]. The two sets of parallel wires cross in the top view of the hole of the cuboid, and form a number of node points as shown in Fig. 3.4. The nodes have been numbered in the same way the data would start coming on the P.C. The format of data acquisition is explained in the section 3.7. The precision of the measurement is directly dependent upon the number of these node points

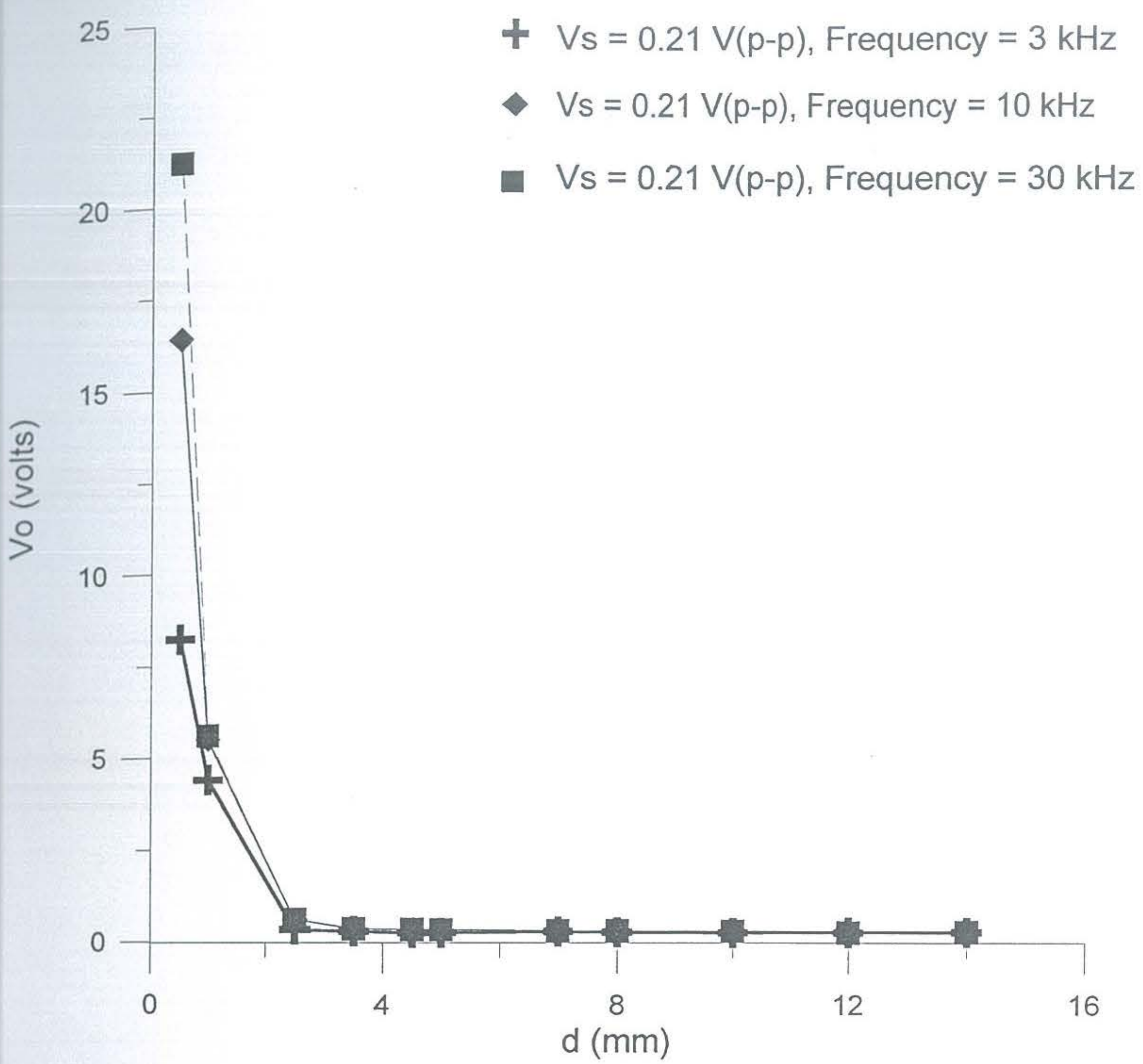

Fig. 3.2. V_o vs d plot

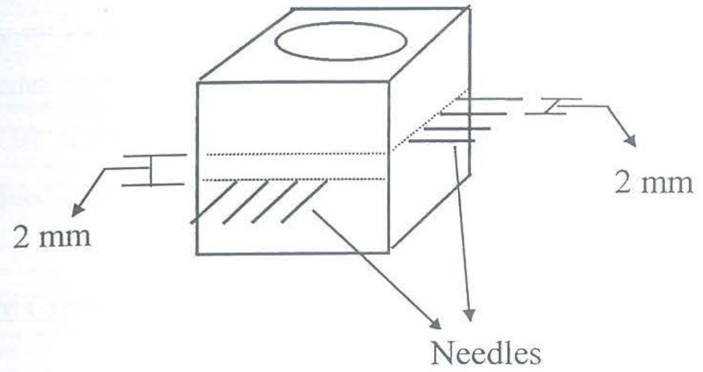

Fig. 3.3. Electrode assembly in the cuboid block

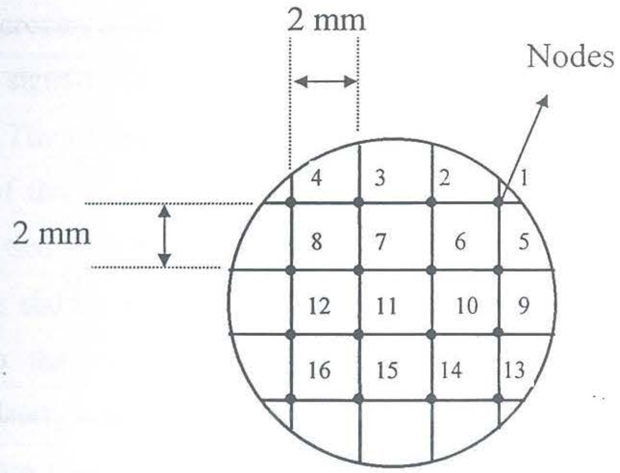

Fig. 3.4. Top view of the electrodes through the hole in the cuboid block. Node numbers are references for data collection

among other factors. The present assembly was restricted to 4 wires, primarily due to the considerations of cost, and ease in fabrication of the mechanical assembly. Steel wires were chosen because of their strength, and non-corrosive properties. These are important considerations because some of the two-phase flows (water–air, water-steam, etc) can be very corrosive. Also since the distance between the wires is of the order of mm, they should not bend and touch each other. Apart from this assembly, there were other mechanical components used for the complete set-up. This is explained in the next chapter.

3.3 Electronic Circuit for Probe

A block schematic of the electronic circuit is shown in Fig. 3.5. The generation of excitation, and acquisition of the measured values is handled by the microcontroller. Four electrodes are excited, one at a time, by the pulses generated by the microcontroller and buffered by the unity gain amplifier. For each excitation, signals on all the four sensing electrodes are sensed by the I/V converters. The converter is used to scale the output so that it is in the range of operation of the ADC. In the present application the clock inputs of all the four ADC's are tied together. The timing diagram for the scanning of one excitation electrode is shown in Fig. 3.6. The signal from the four receiving electrodes in response to the excitation pulse is sensed simultaneously. The ADC selected (described later) needs five clock pulses "ck" for conversion. At the first clock, all the inputs are sampled, and at the fifth clock the values become available at the output latch. The outputs remain disabled during this interval. After the outputs have become available, these are read by feeding enable pulses "en", generated by microcontroller, one by one to the four ADC's.

The above process is repeated for other three electrodes in the grid. At the end of four cycles, sixteen data values get stored in the microcontroller. These are transmitted serially to a PC. The timing diagram for scanning the four electrodes,

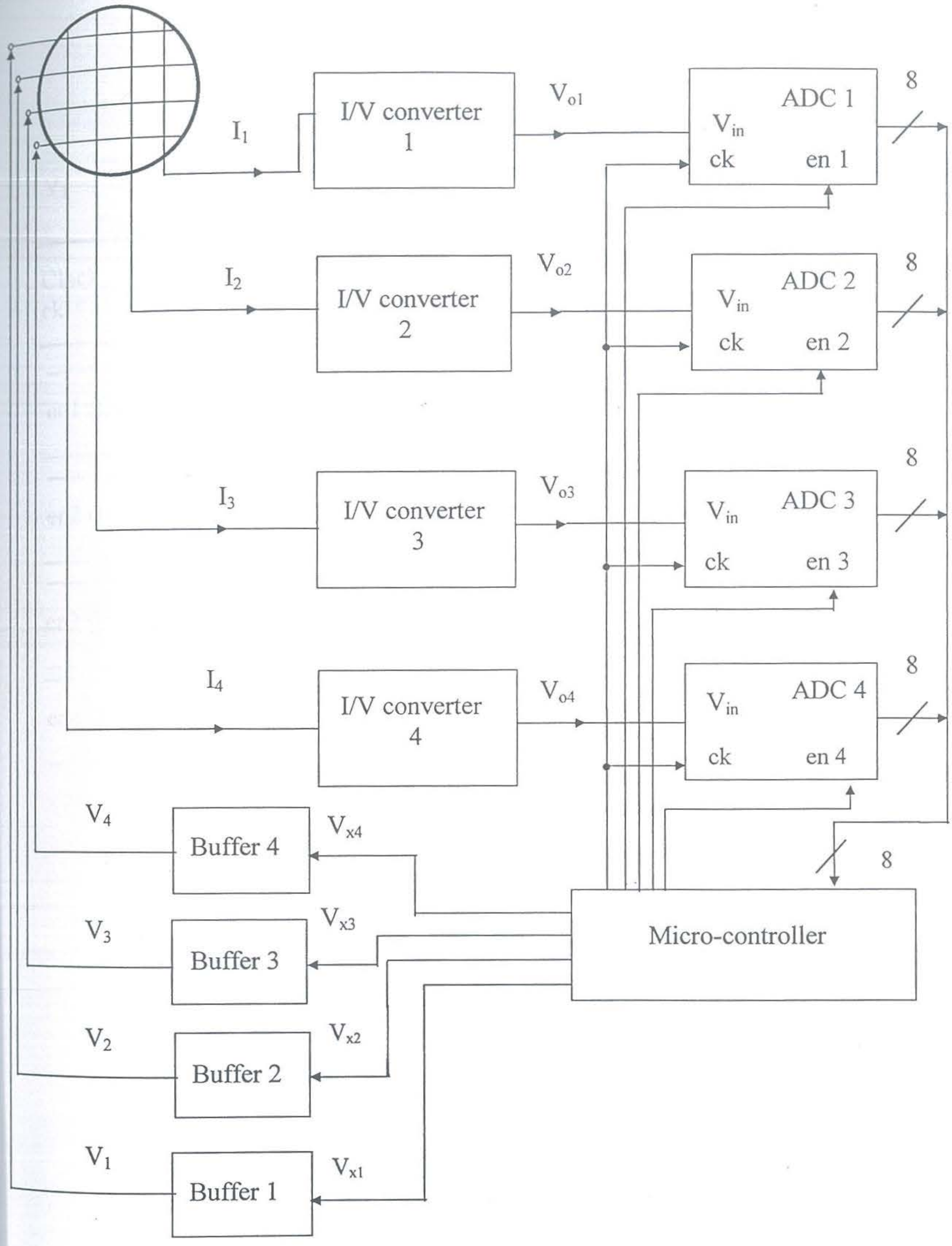

Fig. 3.5. Block diagram of the electronic circuit

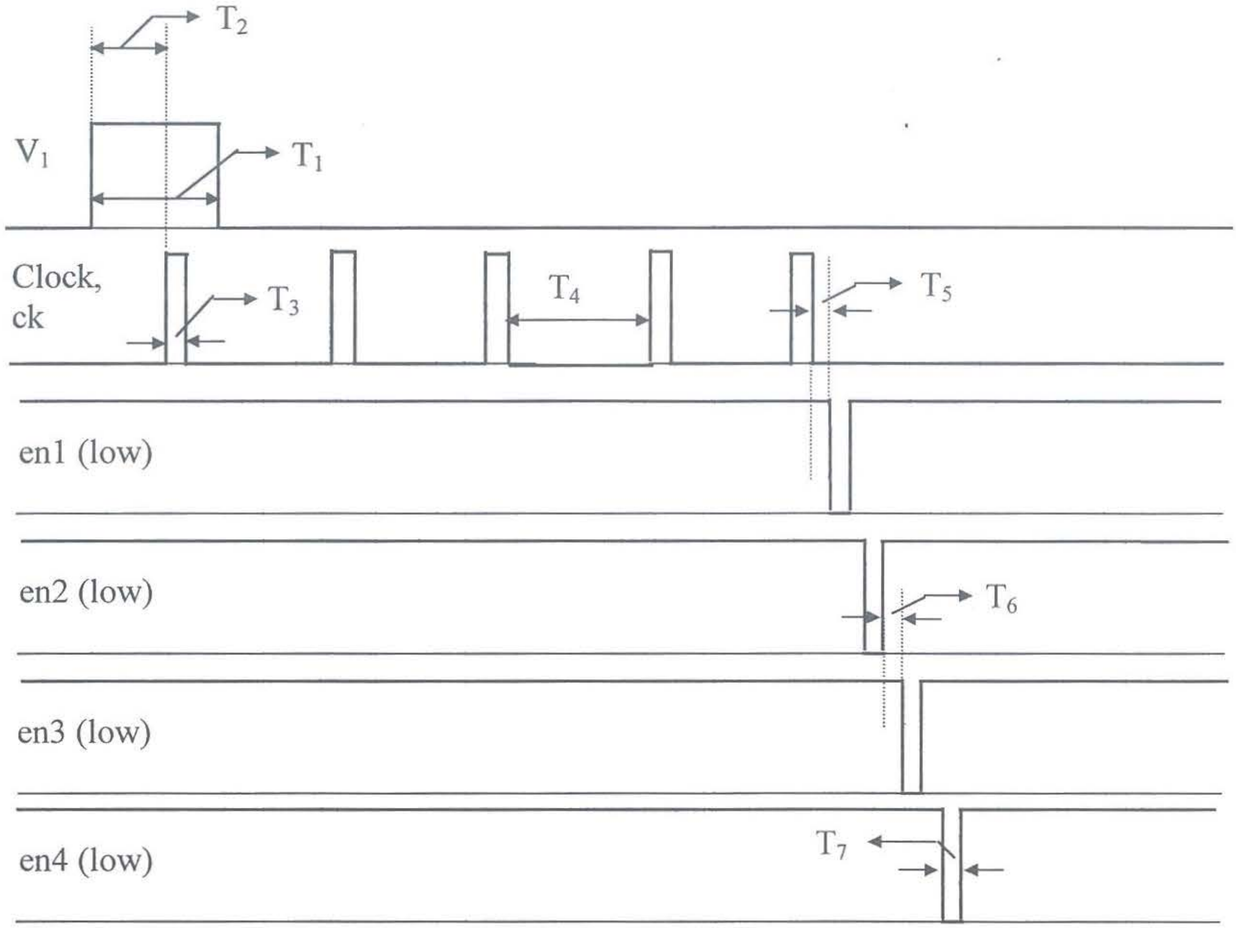

Fig. 3.6. Timing diagram for channel 1
$T_1 = 24\ \mu s$, $T_2 = 15\ \mu s$, $T_3 = 2\ \mu s$
$T_4 = 15\ \mu s$, $T_5 = 2\ \mu s$, $T_6 = 2\ \mu s$
$T_7 = 2\ \mu s$

and data transmission is shown in Fig. 3.7. After the data acquisition is over, a program on the PC is used to process the data to get the necessary information on void fraction.

3.4 Circuit Blocks

The overall block diagram of the electronic circuit is shown in Fig. 3.5 and described in the previous section. In this section the individual blocks of the circuit are described. The consideration for the selection of components is also presented.

1. Buffer Amplifier and I/V Converter

The excitation pulses, generated by the microcontroller, are buffered by using unity follower as a buffer amplifier shown in Fig. 3.8. In Fig. 3.8 is, also, shown the I/V converter that gives an output voltage inversely proportional to the impedance offered between the electrodes (Section 3.1). The opamps needed for the buffer amplifier and the I/V converters needed to have high slew rate for fast pulse response. In addition, the opamp used for the I/V converter should have low input bias current. A large input bias current would cause a D.C error. Opamp LF351 was chosen for both the circuits, based on the considerations of availability, and cost [15]. This opamp has an input bias current of 50 pA and a slew rate of 13 V/ μs.

For the buffer amplifier, a low-pass filter formed by R1, and C1 has been used with a time constant of 1.2 μs. The time constant is much smaller than the excitation pulse width of 24 μs. It has to be noted that the excitation pulses are generated by the microcontroller and there are narrow glitches due to digital switching. The low-pass filters serve the purpose of smoothening these glitches in

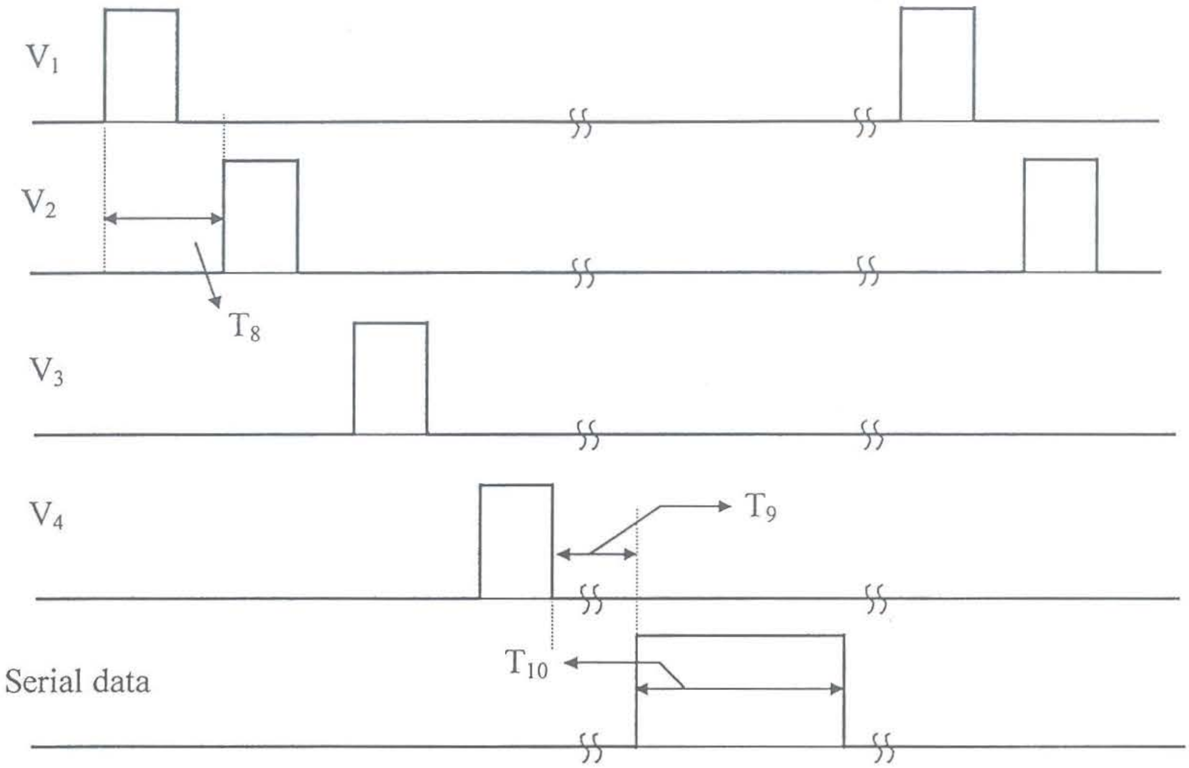

Fig. 3.7. Timing diagram for excitation of the four channels, and data transmission $T_8 = 79\ \mu s$, $T_9 = 10\ \mu s$, $T_{10} = 25$ ms

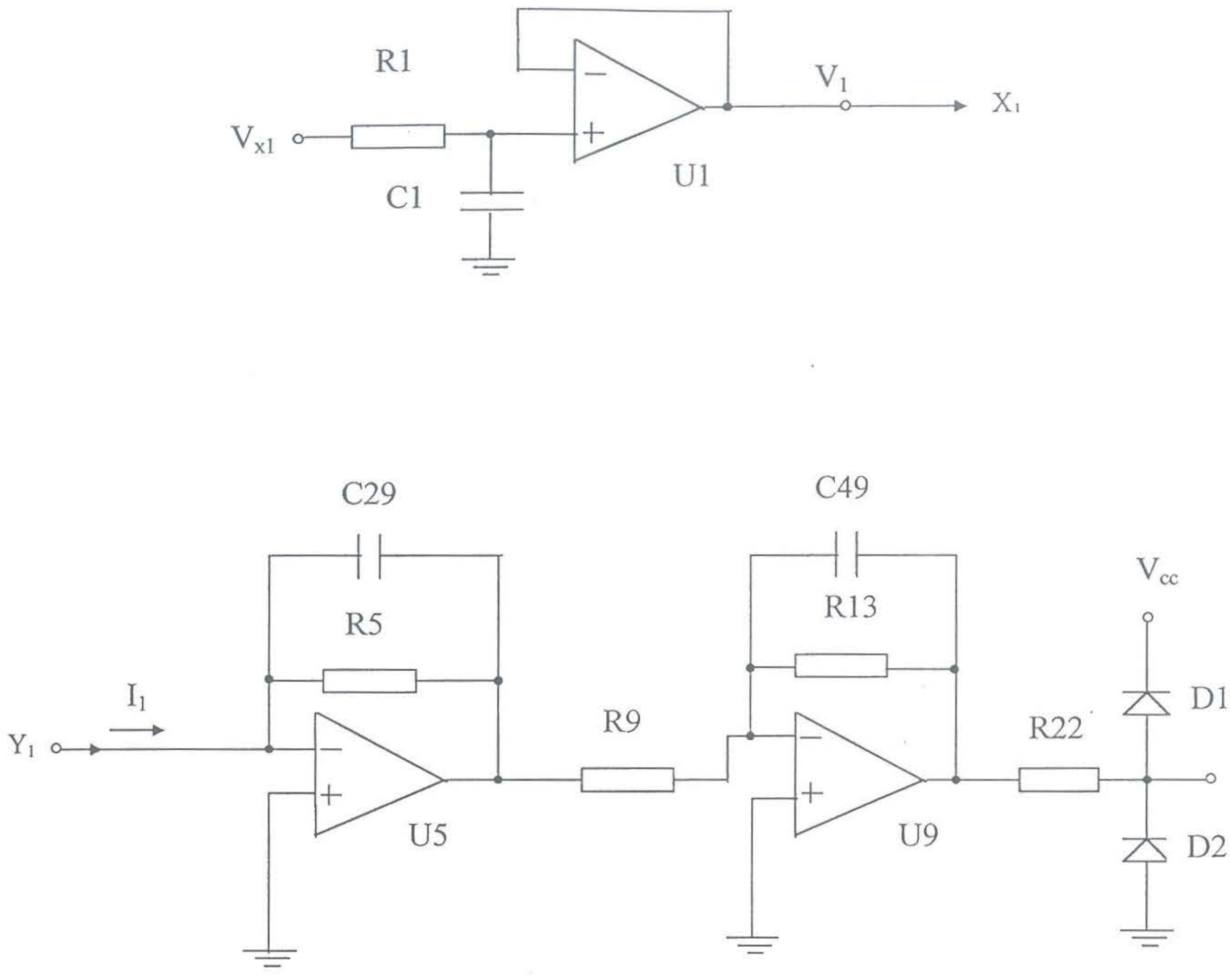

Fig. 3.8. Buffer amplifier and circuit for I/V converter
U1, U5, U9: LF351
R1 = 100 k ohm, C1 = 12 pF
R5 = 6.8 k ohm, C29 = C49 = 22 pF
R9 = R13 = 38.4 k ohm, R22 = 68.2 ohm
D1, D2: IN4007

the input pulse, and to make the inputs to unity gain buffer amplifiers referred to the analog ground.

The I/V converter has two stages. First stage has a sensitivity of 6.8 V/mA and a time constant of 0.1496 μs. The second stage is an inverting amplifier with a gain of one and time constant of 0.8448 μs. Thus the I/V converter gives an output pulse of 2.6 V for a current pulse of 0.38 mA. The output of the inverting stage is given to an output limiting circuit consisting of resistor R22, and diodes D1 and D2. This ensures that the input to ADC will be limited in the 0 – 5 V when the supply, $V_{cc,}$ is of 5 volts.

2. Analog- to- Digital Converter

Two important features that were required for an ADC chip are an in-built sample-and-hold (S/H) input, and a tri-state output buffer. With these two features, all the inputs can be sampled simultaneously (common clock, ck, for the four ADC's) and after the A/D conversion, the digital outputs of the ADC's can be put on the 8-bit bus one after the other using the enable facility. Extensive survey of various ADC's was done from the available data as well as from internet. It was decided to use EXAR MP8786 [16] that suited our requirement. It is an 8-bit cascaded flash converter (a brief description is given in Appendix A) with internal S/H function. It requires five clock pulses. The first pulse is used to track the input using S/H and the conversion process of this sampled input requires four pulses one each for conversion, latch, encoding and error correction, and output latch. This ADC can be used with a maximum sampling rate of 30 MHz.

3. Microcontroller

The features that were looked into a microcontroller to be used were the speed of the processor, and the availability of suitable number of sets of ports to generate input pulses, clock pulses, and the enable signals for the ADC's. Also a timer facility, which would be utilized in the serial transmission of the stored data, was required. These considerations along with easy availability and pricing made Atmel AT89C52 [17] a suitable choice for the project. The ADC's and micro-controller were connected appropriately and tested for serial transmission of data. The microcontroller operates on +5 V supply. It has four 8-bit data ports: P0, P1, P2, P3. The pins of port P3 have dual functions like I/O, serial data transmission, interrupt, etc. The microcontroller is operated using 11.0592 MHz crystal. This frequency helps in precise setting of the transmission rate at 2400, 4800, or 9600 bps (bits per second). The port pin assignment of the microcontroller is shown in Fig. 3.1. Port P0 of the microcontroller requires external pull-up resistors for pulse generation. The pull-up resistors have been designated as R17 –R21. Each resistor has a value 1.2 k ohm.

4. I.C. for Serial Transmission

For the serial transmission of data the microcontroller output is connected to ADM232 as an RS-232 driver for compatibility with the PC. ADM232 operates on a 5 V supply.

3.5 D.C. Power Supply

The Integrated Circuits, selected for the project, operate on + 5/0/-5 V supply. The ADC's, micro-controller, and the serial transmission chip need +5 volt supply, while the operational amplifiers operate on +5/0/-5 V. A regulated power supply providing the required voltage levels is shown in Fig. 3.9. A 230/9-0-9 V transformer is used at the input. Full wave rectified wave is obtained after the bridge rectifier at the input of the regulator chips. A 470 μF capacitor is used at the input of regulators to smoothen the rectified wave. At the output of the regulators, a 0.1 μF capacitor is used to filter any high frequency noise.

Table 3.1. Microcontroller port pin assignment

I/O port pins	Function
P 0.0	en1
P 0.2	en2
P 0.4	en3
P 0.6	en4
P 0.7	ck
P 1.0	V_4
P 1.1	V_3
P 1.2	V_2
P 1.3	V_1
P 2.0 – 2.7	ADC data
P 3.1	Serial TXD

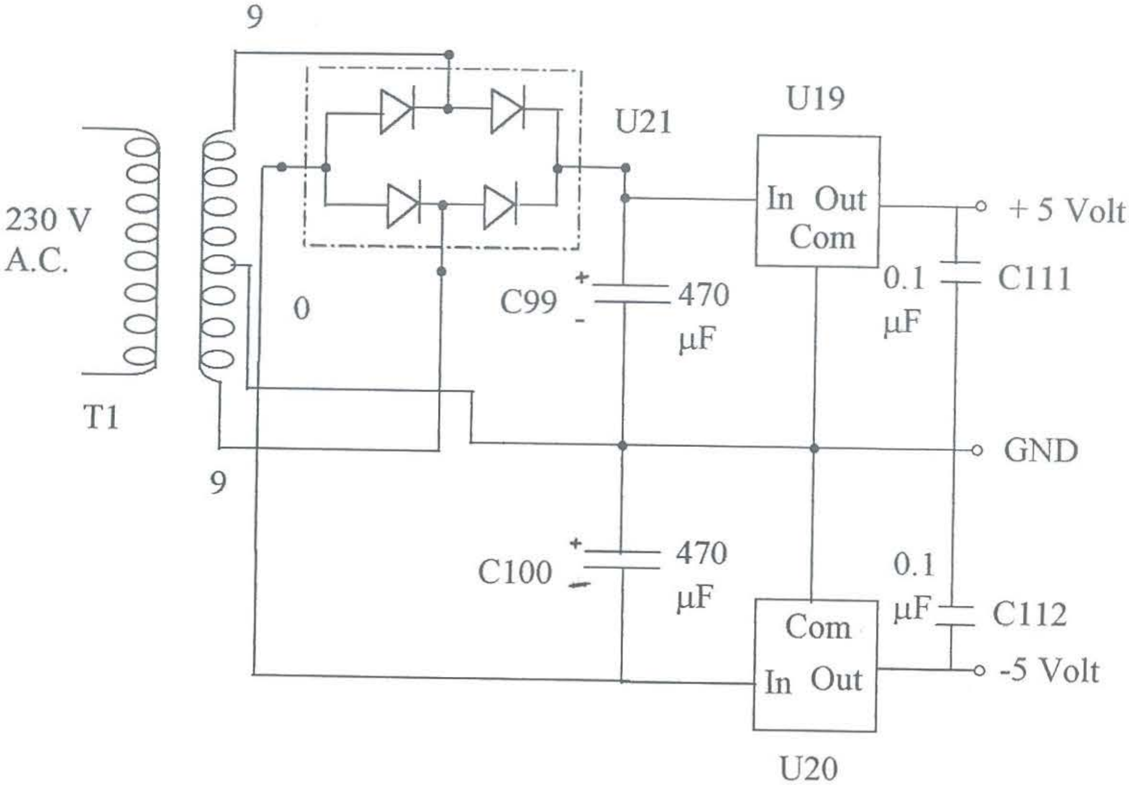

Fig. 3.9. Regulated power supply
T1: 230 V/ 9-0-9 V, 500 mA
U19: LM7805, U20:LM7905,
U21: RB153

3.6 Circuit Assembly

The block schematic diagram for the electronic circuit has been given in Fig. 3.5, and the circuits for individual blocks have been described in the previous section. An overall circuit diagram is given in Fig. 3.10. Decoupling capacitors of value 0.1 μF and 0.01 μF are used across power supply and ground for each of the I.C's. The component values are listed in Table 3.2.

A general purpose PCB was used to make the D.C. power supply. The PCB layout for the main circuit board was done using a PCB layout package. The component placement is shown in Fig. 3.11a. The PCB consisted of two layers, top layer, and the bottom layer as shown in Fig. 3.11b and Fig. 3.11c respectively. The ADC's used in the circuit have separate analog and digital $+V_{cc}$ supply pins. Therefore the analog $+V_{cc}$ ($+AV_{cc}$) of ADC, and $+V_{cc}$ of the operational amplifiers were shorted and a common track for them was present on the top layer. The top layer also had $-V_{cc}$ track ($-AV_{cc}$) for the operational amplifier. The supply lines of the microcontroller, ADC's, and the serial transmission chip ADM232 were shorted and this was made as a separate digital $+V_{cc}$ (DV_{cc}) track on the top layer. The analog and the digital $+V_{cc}$ were shorted at the D.C supply end. On the bottom layer the analog ground (AGND) of the ADC's and ground of operational amplifiers were shorted. Also, the digital ground (DGND) of the four ADC's, micro-controller, and the serial transmission chip ADM232 were shorted. The separate analog and the digital ground tracks were connected at the D.C supply end. The $+V_{cc}$, $-V_{cc}$, and ground tracks have been kept wide for reducing the resistance and inductance of the tracks. All the track lengths were minimized, to the extent possible manually. To minimize noise, decoupling capacitors of value 0.1 μF, and 0.01 μF were connected between the supply pin and ground for each of the IC's as shown in Fig. 3.10.

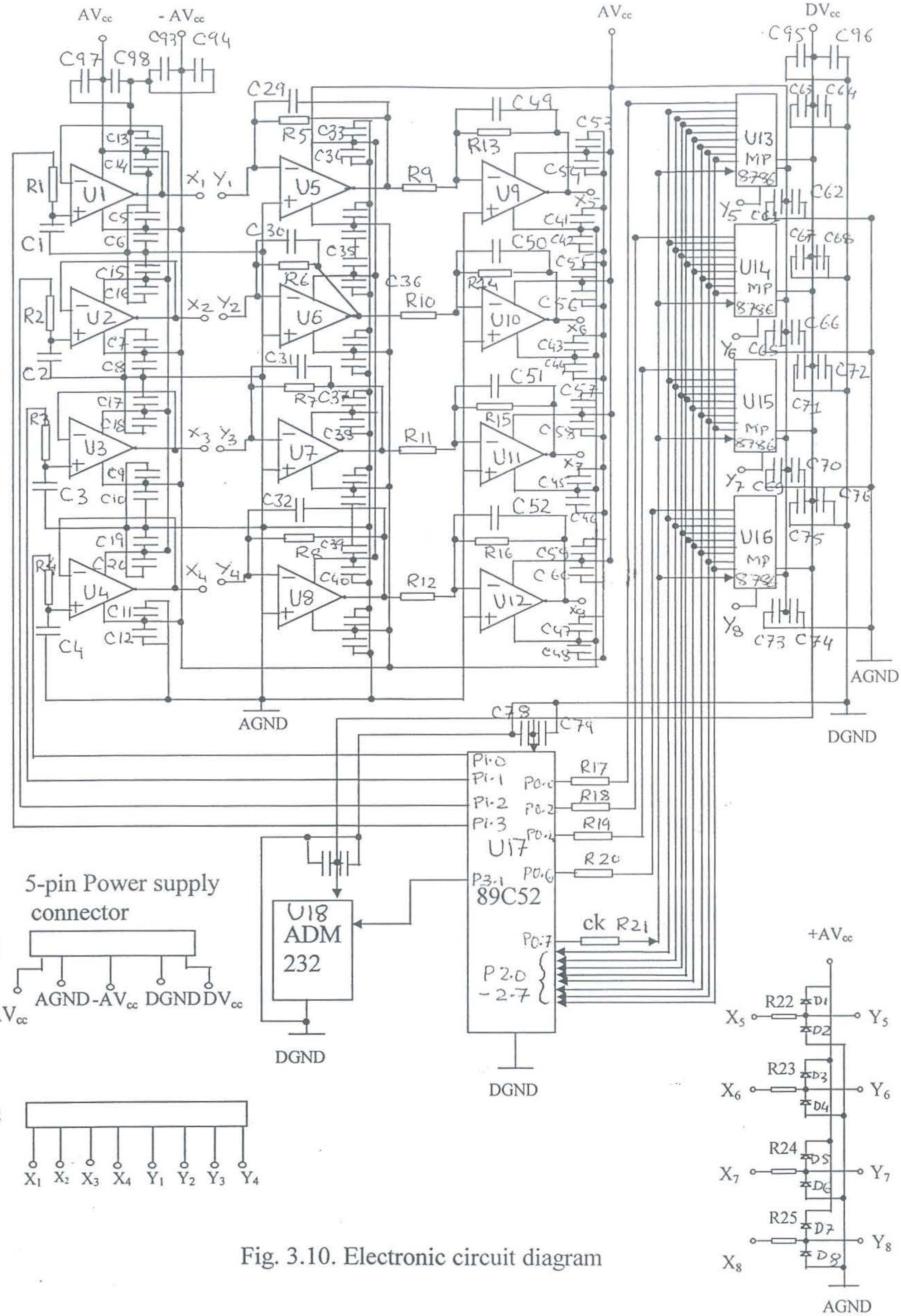

Fig. 3.10. Electronic circuit diagram

Table 3.2. Component values

Reference Designator	Value	Reference Designator	Value	Reference Designator	Value
C1	12 pF	C32	22 pF	C63	0.1μF
C2	12 pF	C33	0.1μF	C64	0.01μF
C3	12 pF	C34	0.01μF	C65	0.1μF
C4	12 pF	C35	0.1μF	C66	0.01μF
C5	0.1μF	C36	0.01μF	C67	0.1μF
C6	0.01μF	C37	0.1μF	C68	0.01μF
C7	0.1μF	C38	0.01μF	C69	0.1μF
C8	0.01μF	C39	0.1μF	C70	0.01μF
C9	0.1μF	C40	0.01μF	C71	0.1μF
C10	0.01μF	C41	0.1μF	C72	0.01μF
C11	0.1μF	C42	0.01μF	C73	0.1μF
C12	0.01μF	C43	0.1μF	C74	0.01μF
C13	0.1μF	C44	0.01μF	C75	0.1μF
C14	0.01μF	C45	0.1μF	C76	0.01μF
C15	0.1μF	C46	0.01μF	C77	10 V, 10 μF
C16	0.01μF	C47	0.1μF	C78	0.01μF
C17	0.1μF	C48	0.01μF	C79	0.1μF
C18	0.01μF	C49	22 pF	C80	63 V, 0.1μF
C19	0.1μF	C50	22 pF	C81	63 V, 0.1μF
C20	0.01μF	C51	22 pF	C82	63 V, 0.1μF
C21	0.1μF	C52	22 pF	C83	63 V, 0.1μF
C22	0.01μF	C53	0.1μF	C84	63 V, 0.1μF
C23	0.1μF	C54	0.01μF	C85	0.1μF
C24	0.01μF	C55	0.1μF	C86	0.1μF
C25	0.1μF	C56	0.01μF	C87	0.1μF
C26	0.01μF	C57	0.1μF	C88	0.1μF
C27	0.1μF	C58	0.01μF	C89	0.1μF
C28	0.01μF	C59	0.1μF	C90	0.1μF
C29	22 pF	C60	0.01μF	C91	0.1μF
C30	22 pF	C61	0.1μF	C92	0.1μF
C31	22 pF	C62	0.01μF	C93	0.1μF

contd…

Reference Designator	Value	Reference Designator	Value	Reference Designator	Value
C94	0.01μF	R8	6.8 k ohm	U5	LF351N
C95	0.1μF	R9	38.4 k ohm	U6	LF351N
C96	0.01μF	R10	38.4 k ohm	U7	LF351N
C97	0.1μF	R11	38.4 k ohm	U8	LF351N
C98	0.01μF	R12	38.4 k ohm	U9	LF351N
C99	25 V, 470μF	R13	38.4 k ohm	U10	LF351N
C100	25 V, 470μF	R14	38.4 k ohm	U11	LF351N
C111	0.1μF	R15	38.4 k ohm	U12	LF351N
C112	0.1μF	R16	38.4 k ohm	U13	MP8786
D1	IN4007	R17	1.2 k ohm	U14	MP8786
D2	IN4007	R18	1.2 k ohm	U15	MP8786
D3	IN4007	R19	1.2 k ohm	U16	MP8786
D4	IN4007	R20	1.2 k ohm	U17	AT89C52
D5	IN4007	R21	1.2 k ohm	U18	ADM232
D6	IN4007	R22	68.2 ohm	U19	LM7805
D7	IN4007	R23	68.2 ohm	U20	LM7905
D8	IN4007	R24	68.2 ohm	U21	RB153
R1	100 k ohm	R25	68.2 ohm		
R2	100 k ohm	R26	8.2 k ohm		
R3	100 k ohm	T1	230 / 9-0-9 V, 500 mA		
R4	100 k ohm	U1	LF351N		
R5	6.8 k ohm	U2	LF351N		
R6	6.8 k ohm	U3	LF351N		
R7	6.8 k ohm	U4	LF351N		

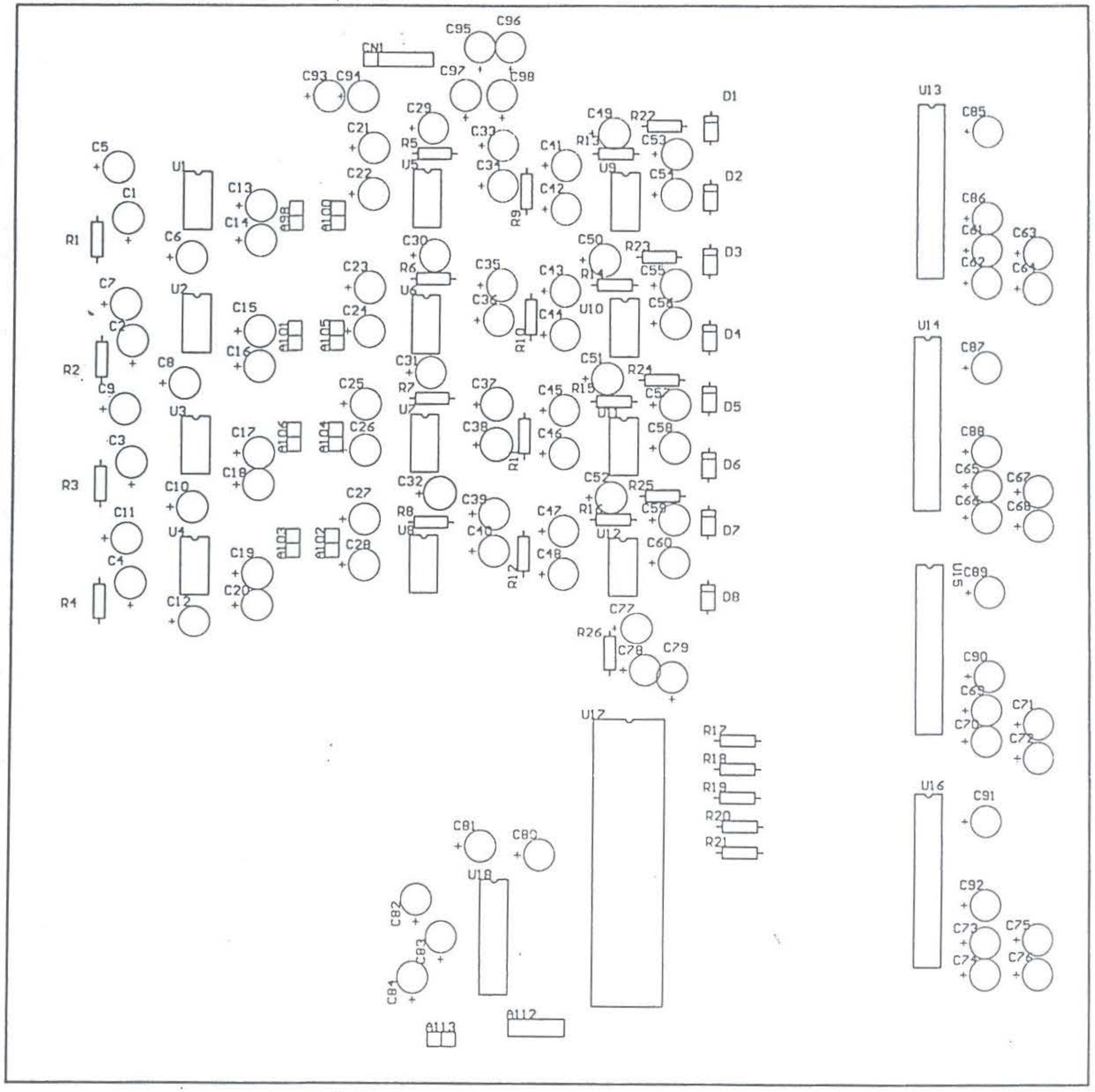

Fig. 3.11a. Component placement for the electronic circuit

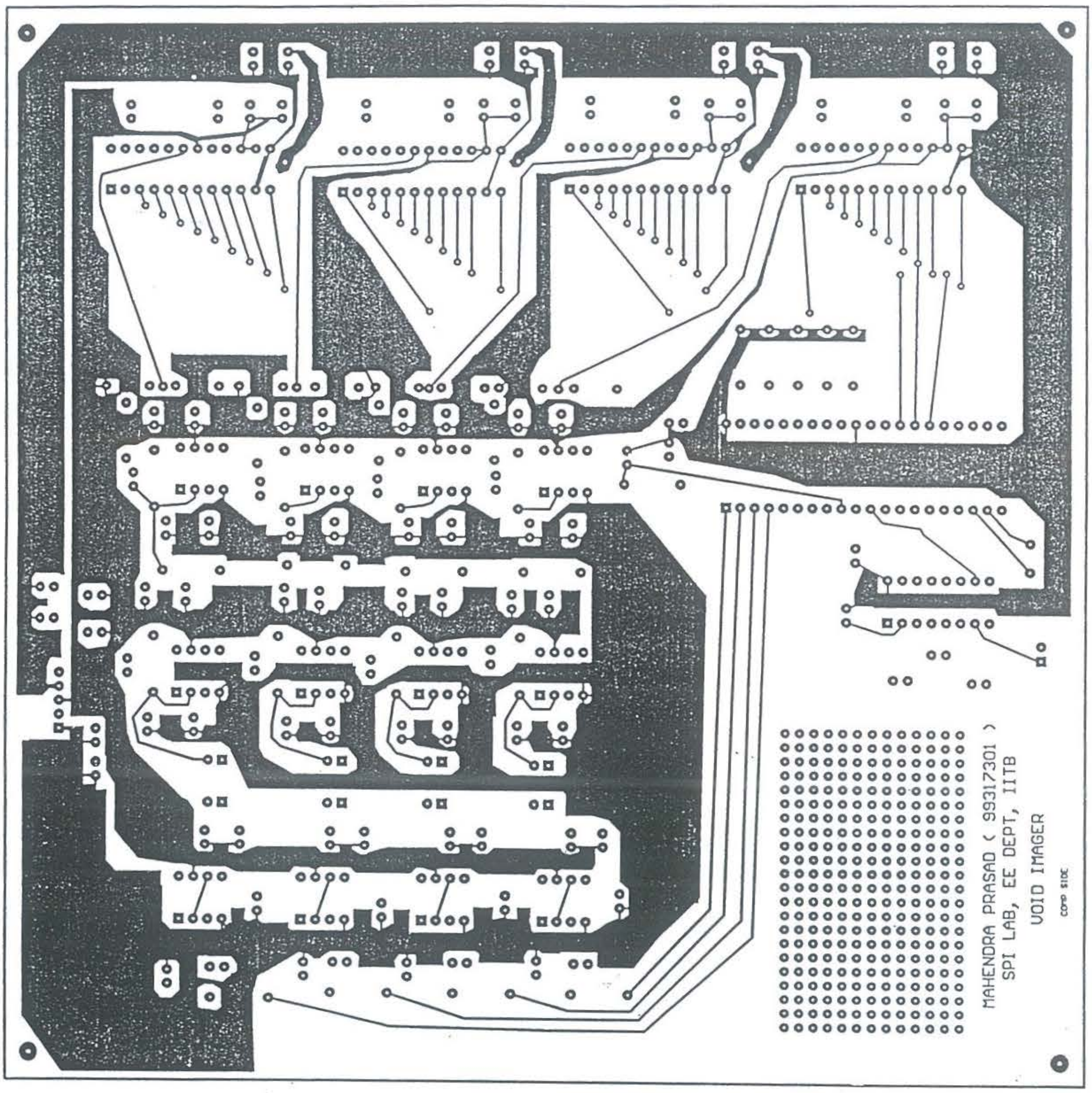

Fig. 3.11b. Top layer of the PCB

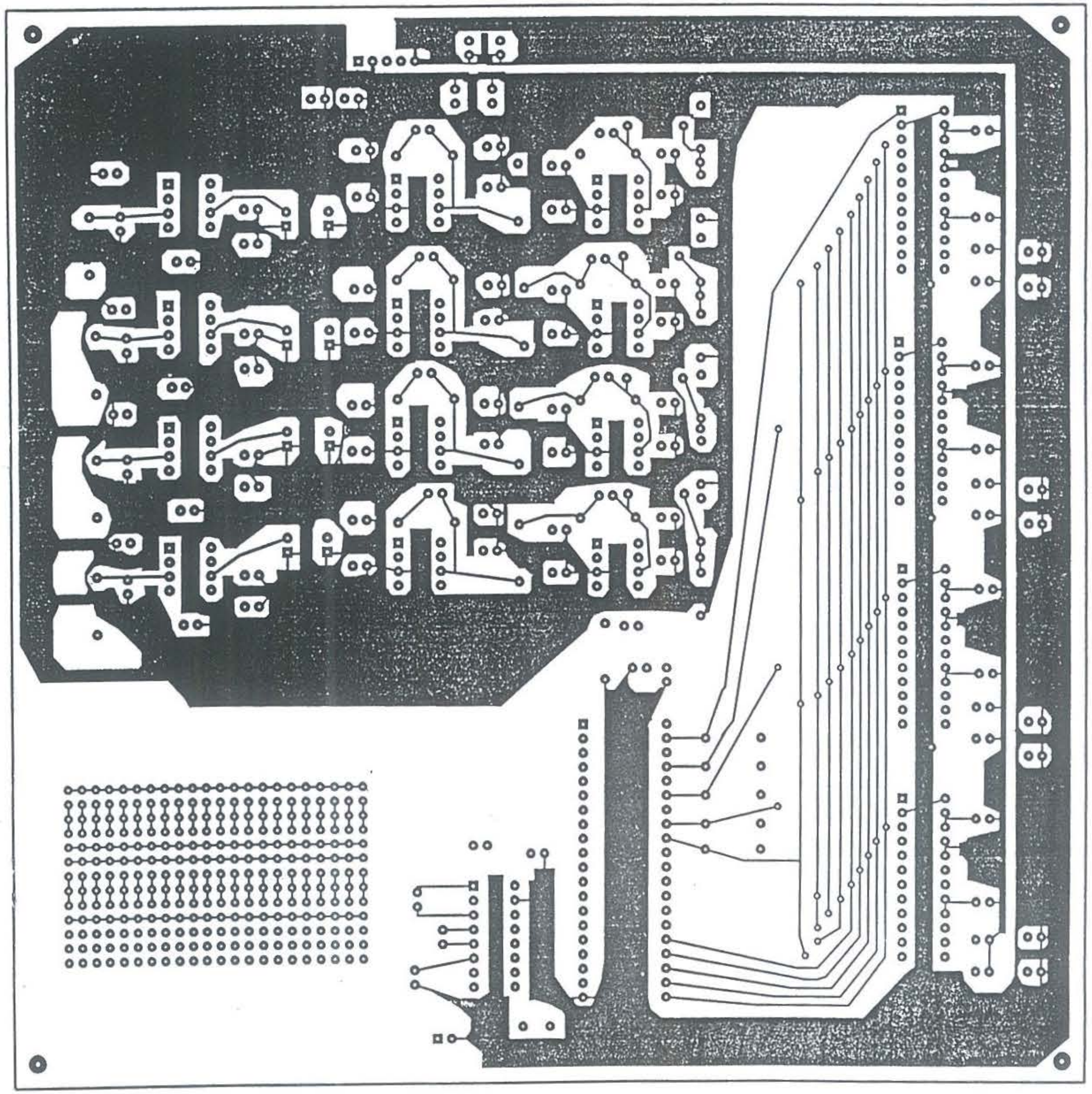

Fig. 3.11c. Bottom layer of the PCB

3.7 Programming

The measurements using the sensor assembly and the electronic circuit are made with the help of a program running on the microcontroller. This program generates excitation pulses, controls the operation of the ADC's, reads the converted data, and at the end of 4 scan cycles transmits the data on the serial link. A program running on the PC is used for receiving the data transmitted by the microcontroller.

The measured values have been constrained in the range 0-247. After each scanning, the microcontroller transmits a synchronizing sequence of 255, 254, 253, 252 to indicate the beginning of a new set of measured values. These are followed by 16 bytes containing actual measured values. The data are again padded with a confirmation sequence of 251, 250, 249, 248. The synchronization and ending byte sequence ensure integrity of data transmission between the microcontroller and the PC. The entire data sequence is

255, 254, 253, 252, $<DX_1Y_1>$, $<DX_1Y_2>$, $<DX_1Y_3>$, $<DX_1Y_4>$, $<DX_2Y_1>$, $<DX_2Y_2>$, $<DX_2Y_3>$, $<DX_2Y_4>$, $<DX_3Y_1>$, $<DX_3Y_2>$, $<DX_3Y_3>$, $<DX_3Y_4>$, $<DX_4Y_1>$, $<DX_4Y_2>$, $<DX_4Y_3>$, $<DX_4Y_4>$, 251, 250, 249, 248.

The program running on the PC receives the 16 data bytes valid only if they are preceded by correct start bytes and followed by correct ending bytes. The transmission is carried out at 9600 bps. A single byte transmission on the serial line requires one start bit, and one stop bit. Thus to transmit 24 bytes (16 actual data and 8 synchronizing bytes) for one scan, a total of 240 bits needs to be transmitted. The time to transmit 24 bytes is, therefore, 25 ms. The next section describes testing of the electronic circuit, and the data acquisition software under static conditions.

3.8 Testing of the Probe System

For testing of the probe system, a circuit model of the sensor assembly in a two-phase flow, as shown in Fig. 3.12, was used. X_1, X_2, X_3, X_4 are the excitation electrodes and $Y_1, Y_2, Y_3,$ Y4 are the sensing electrodes. The impedance Z_{ab} in the circuit represents the impedance between excitation electrode X_a and sensing electrode Y_b. The impedances used were resistors of value 22 k ohm . All the sixteen sensed values were found to be approximately equal. No significant random variations were observed, indicating that noise did not affect consistency of the measurement. The testing was repeated for other resistor values.

As the next step, the electronics was connected to the cuboid sensor assembly. One end of the cuboid was plugged with a rubber cork and it was, then, filled with tap water such that the two sets of parallel wires were completely covered with water. All the data were not of the same value, as earlier, because in reality, the distance between the two sets of parallel wires would not be precisely 2 mm. The data obtained from the testing were in the range of 80-110. To simulate a bubble, insulating wires of diameter 1 mm and 2 mm were inserted in the 2 mm x 2 mm square area as shown in Fig. 3.4. The outputs of the nodes, that formed the corners of the square, changed drastically to very low value of around 005-010 as seen on the PC. In fact, when the cuboid was tilted at various angles to prevent water contact at some of the nodes, the output was similar to inserting the wires, i.e, low at some of the nodes. This experiment showed that the circuit was able to capture any variation in the impedance between the two sets of wires and thus, could distinguish between water phase and the gas phase. After having completed the static testing, the electronic circuit was used for the actual condition of two-phase flow in a pipe. This is explained in the next chapter.

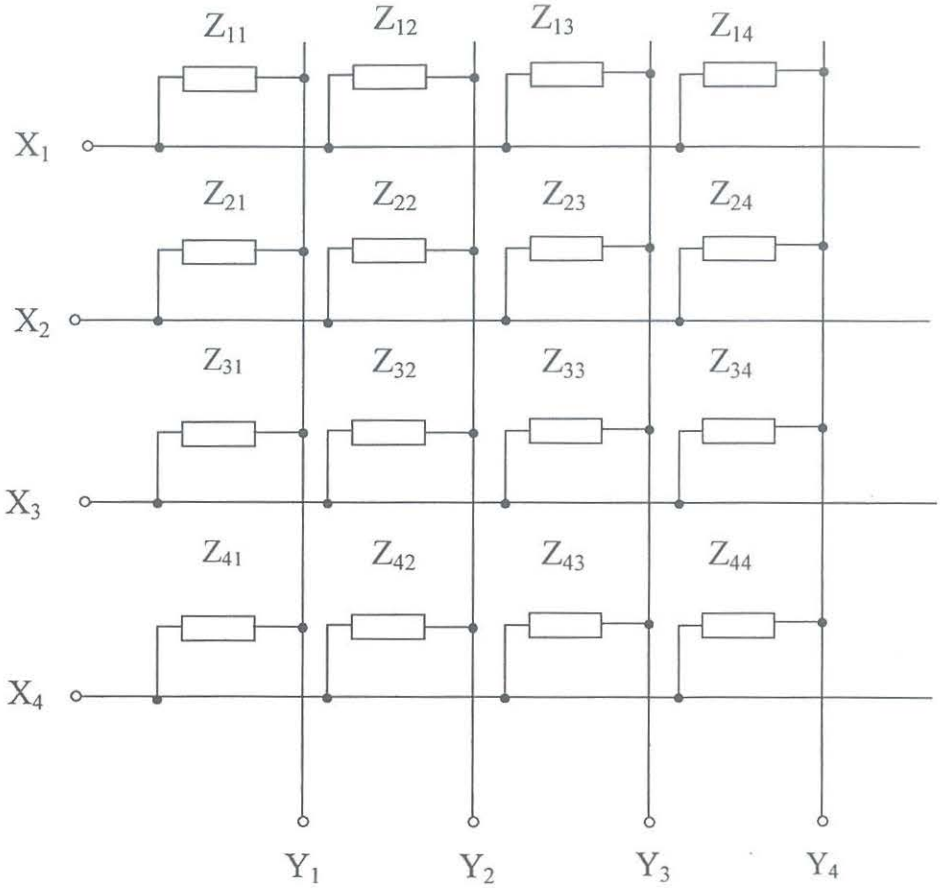

Fig. 3.12. Circuit model of the sensor assembly

Chapter 4

EXPERIMENT ON VOID MEASUREMENT

The previous chapter had presented a detailed description of the mechanical assembly, and the electronic circuit to be used for the development of void probe system. The mechanical assembly, and the electronic circuit were configured suitably and experiments performed for the determination of void fraction. This void fraction value was compared with one measured by a Differential Pressure Transducer (D.P.T.). This is presented in the following paragraphs.

4.1 Cross-Sectional Frames for a Bubble

Fig. 4.1 shows the schematic of the void measuring system. A cylindrical tube of internal diameter 19.5 mm, and external diameter 24 mm was used in a vertical position. The height of the tube was around 75 cm. A cuboid, with a hole of the external diameter of tube as was shown in Fig. 3.3, was coupled with the cylindrical tube. A nitrogen cylinder was used for the generation of bubbles in the tube. For the purpose of regulating the flow of nitrogen and water, valves were provided in the connecting tubes. The receiving, and the transmitting wires of the mesh were connected to the main circuit board by 2 pin-connectors. The circuit was powered by the D.C. power supply as described in Section 3.5.

Water was filled in the cylindrical tube up to the top level of the tube. Nitrogen was, then, passed into the tube at the bottom with its flow regulated by the nitrogen valve. The pressure was sufficiently high to create elongated ellipsoid bubbles called Taylor bubbles as shown the Fig. 4.1. When these bubbles passed through the wire mesh, they acted like a very high impedance path for the current because of which the output seen on the PC was low (this was obtained in the decimal form, range being 0-255). The output on the PC was taken as 4 synchronizing sequence data, 16 actual data from the experiment, 4 confirmation sequence data,

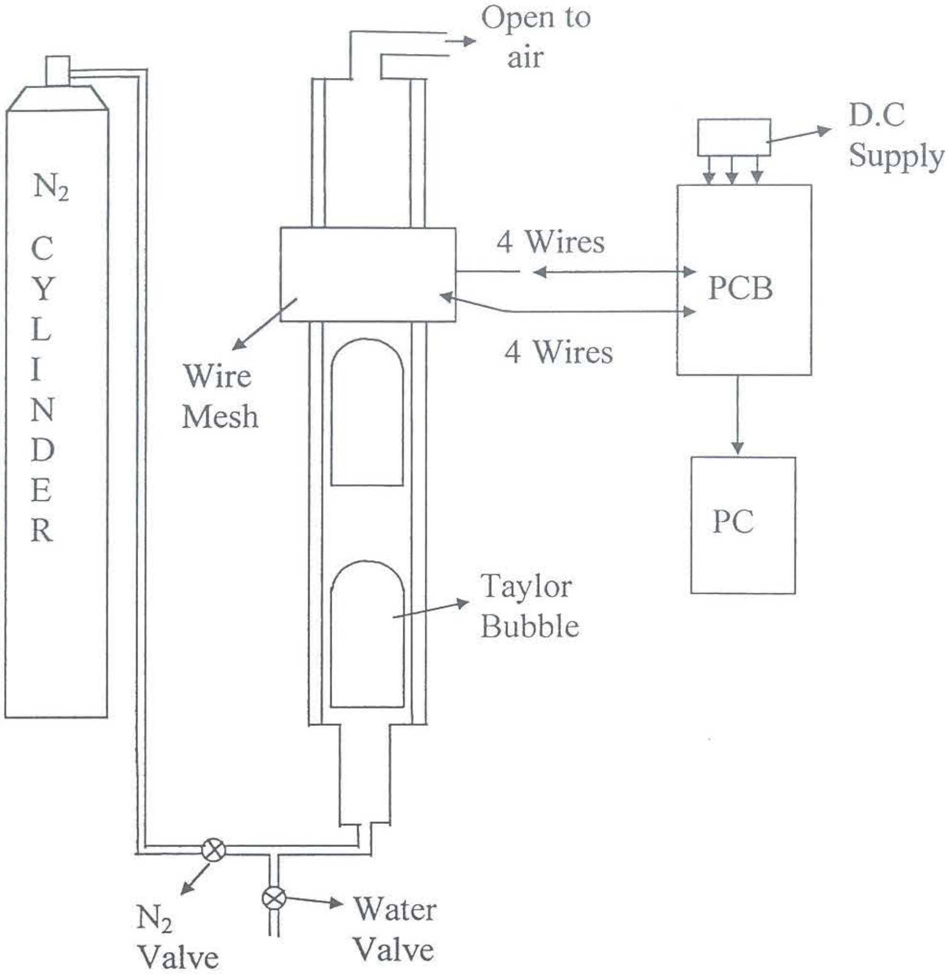

Fig. 4.1. Schematic of the complete set-up

and the corresponding time for the 24 data in one row. For convenience the synchronizing sequence data, and the confirmation sequence data have been referred as marker data in the later part of this section. The reason for the use of marker data was explained in the previous chapter. Output, in the given format, was repeatedly taken for the time the experiment was carried out. The data were taken, usually, for a period of 20-30 seconds. Since the data transfer rate chosen was 9600 bps, the numbers of rows of data collected were around 450-500.

Fig. 4.2 gives a sample data output for a Taylor bubble moving in the pipe. As one can observe the zeroes in the output begins around the central portion of the tube and then, the entire node outputs become zero. The numbers 255, 254, 253, 252, and 251, 250, 249, 248 are the marker data. The marker data have been provided to identify the start and end of the actual data. The data after 252 is the first data (data node 1; the nodes have been numbered in the same way the data is coming on the PC as can be seen from Fig. 3.4; for convenience, the marking of the nodes is shown again in Fig. 4.4.) and after the last data (node 16) 251 appears. The time, t, shown after 248 gives the time for transmitting 24 bytes. The first row has zeroes at node points 6, 7, 10, and 11. The next row has zeroes at the nodes 2, 3, 5, 6, 7, 8, 9, 10, 11, 12, 14, and 15. Subsequently all the nodes have value zero in the next 6 rows. After 24 bytes of data on the screen, the next set of data is received. This is repeated for the time of the experiment. For the bubbles, generated at a particular nitrogen pressure, the data obtained were similar to that shown in Fig. 4.2 except in the initial 2-3 rows when the bubble is more or less spherical (Taylor bubble in Fig. 4.1.). The data after 2-3 rows matched perfectly when the bubbles become fully cylindrical and cover the area around the 16 nodes. The reason for this kind of output would be discussed in next chapter

A software was developed to obtain frames (view of the cylindrical tube cut horizontally) using the data collected for the bubbles as the bubbles passed through the probe section. In the software the actual data, shown in Fig. 4.2, were

Start of the bubble: t = 0.000000
255 254 253 252 091 032 050 065 030 000 000 019 006 000 000 016 033 037 025
022 251 250 249 248 t = 0.054945
255 254 253 252 112 000 000 080 000 000 000 000 000 000 000 000 009 000 000
010 251 250 249 248 t = 0.109890
255 254 253 252 000 000 000 000 000 000 000 000 000 000 000 000 000 000 000
000 251 250 249 248 t = 0.164835
255 254 253 252 000 000 000 000 000 000 000 000 000 000 000 000 000 000 000
000 251 250 249 248 t = 0.219780
255 254 253 252 000 000 000 000 000 000 000 000 000 000 000 000 000 000 000
000 251 250 249 248 t = 0.274725
255 254 253 252 000 000 000 000 000 000 000 000 000 000 000 000 000 000 000
000 251 250 249 248 t = 0.329670
255 254 253 252 000 000 000 000 000 000 000 000 000 000 000 000 000 000 000
000 251 250 249 248 t = 0.384615
255 254 253 252 000 000 000 000 000 000 000 000 000 000 000 000 000 000 000
000 251 250 249 248 t = 0.439560 (end of the bubble)
255 254 253 252 094 028 047 067 027 061 029 016 042 030 024 012 029 034 023
028 251 250 249 248

Fig. 4.2. Sample data for a bubble

compared with certain fixed values called the discriminating values. The meaning of such a discriminating value is that any data larger than this value would represent water while a lower value would represent air. The concept of the discriminating value is important because it could be observed that the numbers 006 and 009, that appear in the data, are very close to 000 and might represent air, or water. An experiment was performed to decide upon the discriminating value for each of the nodes. In the experiment the cuboid block was coupled to the electronic circuit, and water was filled into it. One end of the block was plugged with rubber cork. Then, using a hypodermic needle, water was slowly pulled out. As the water level starts falling down in the measuring volume, the output decreased monotonically to a very low value. At a given instant, when the water film between the wires ruptured, the output instantly decreased to zero. The monotonic decrease in the output voltage is shown qualitatively in Fig. 4.3. This means that a value has to be set for a node, in the wire mesh, to make sure that when an output in the actual experiment on two-phase is below this set value air is present in a volumetric region around that node. The discriminating values were chosen to be half of the values obtained in the static test for the 16 nodes as shown in Fig. 4.3. In the software actual data that were greater than the discriminator value were assigned a value 1 and those smaller than the discriminator value were assigned a value 0. Thus an output, shown in Fig. 4.2, was converted to an output consisting of 1's, and 0's. Assuming symmetrical distribution of a bubble round a node point, for a data with value zero a square of size 1 mm x 1 mm was plotted to represent nitrogen (gas phase) around the corresponding node point. Everywhere else the plot represented water (liquid phase).

Fig. 4.4 shows the pictorial representation of the data obtained for a bubble. As shown in Fig. 4.2, the data for the nodes 6, 7, 10, and 11 was zero in the first row (frame 1). The next row had data for nodes 2, 3, 5, 6, 7, 8, 9, 10, 11, 12, 14, and 15 as zero (frame 2). Subsequently, all rows had value zero for all the 16 nodes. The central portion in the Fig. 4.4 shows void (nitrogen), as the bubble tip touches and

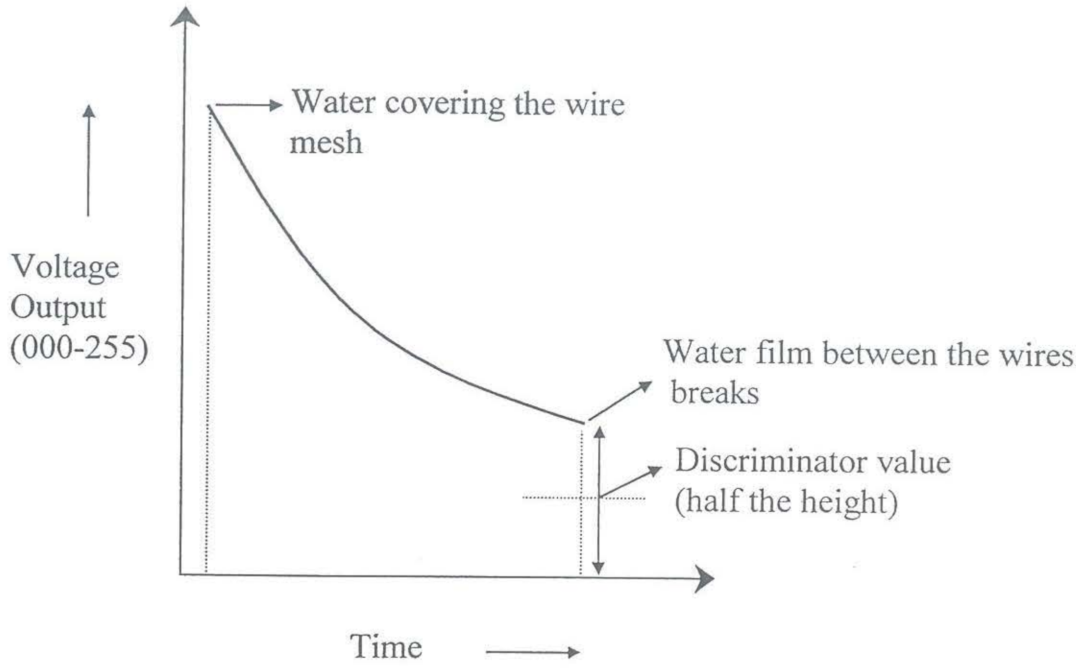

Fig. 4.3. Qualitative representation of the decrease in voltage output when water is pulled out of the cuboid block

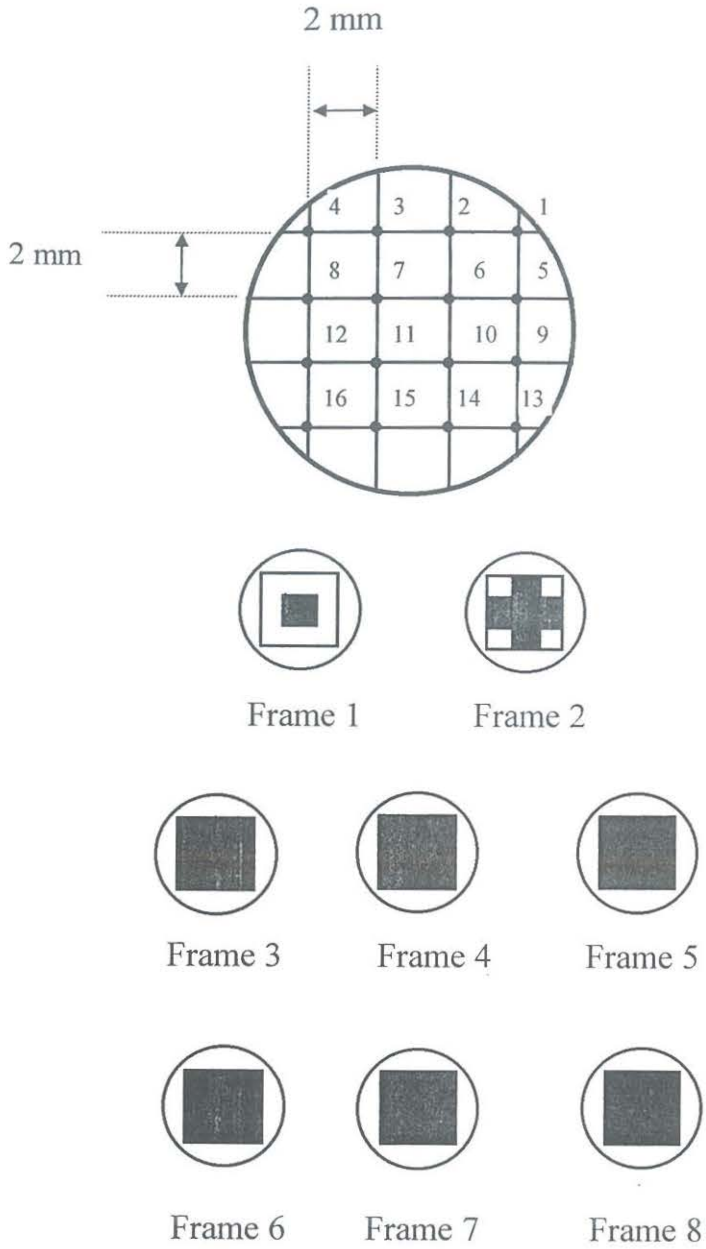

Fig. 4.4. Cross-sectional frames

crosses the wire mesh. Thereafter, due to the cylindrical nature of the bubble, whole of the area around the 16 nodes (the points where the 4 wires in each set seem to cross in the top view of the cuboid block) give the void representation. The time elapsed between each of the frames was around 55 ms. From the pictorial representation, cross-sectional views about lines formed by nodes 4, 8, 12, and 16 (the first line from left in Fig. 4.4); 3, 7, 11, and 15 (second line); 2, 6, 10, and 14 (third line); 1, 5, 9, and 13 (fourth line) was plotted using MATHEMATICA. This is shown in Fig.4.5. The gap between any two lines in the any of the perspective views is representative of the distance travelled by bubble in the time required to get one frame (total 24 data on PC). This gives a rough image of the bubble, even though the data is not sufficient enough to get a very clear picture. The void measuring system demonstrated that it could distinguish between the two components of a two-phase flow when the components had significant differences in electrical properties (water and nitrogen) and give an approximate volumetric image of the gas phase. After this, experiments were performed to compare length of a Taylor bubble as obtained by the data acquisition with that by observation.

4.2 Bubble Mapping

Nitrogen was passed in the tube with sufficiently high pressure to generate elongated Taylor bubbles. The bubbles were approximately of the same length over the period of experimentation. Two marks were made on the outer surface of the tube. The marks were at a distance of around 21 cm. The time, elapsed between the instants when the tip of a Taylor bubble moving up touched the two marks, was recorded. A third mark was also made on the surface. The purpose of this mark was to get the time taken for a bubble to cross this mark. The time would be related to the length of the bubble. In Fig. 4.6 is shown the schematic to calculate the bubble length, and velocity. The first reading for each bubble gave the information about its speed.

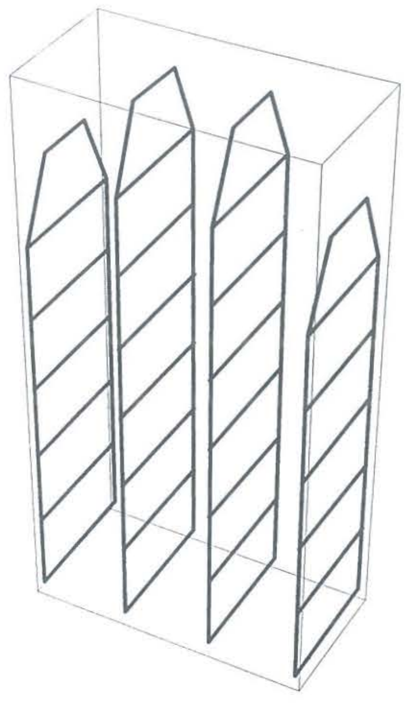

Perspective View

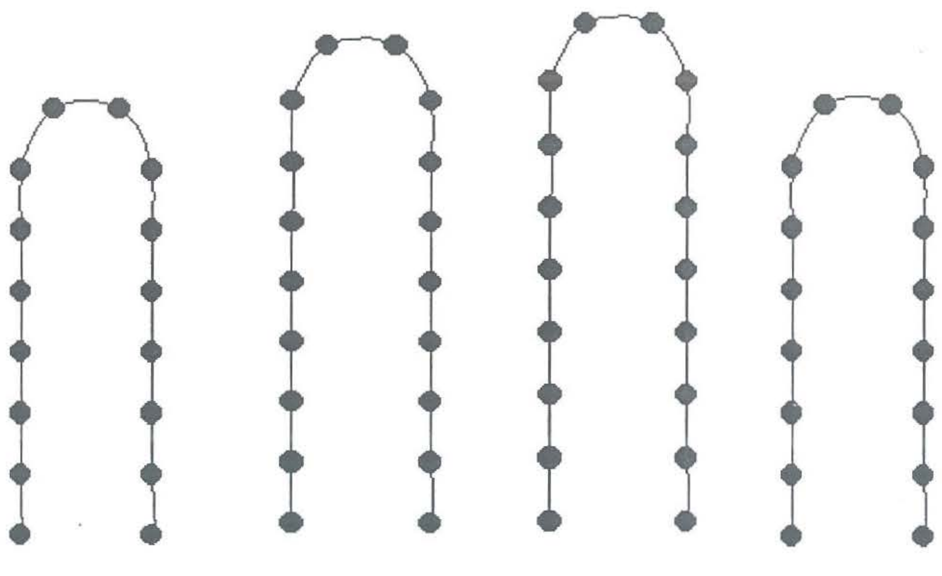

Fig. 4.5. Sectional views along the length of a bubble

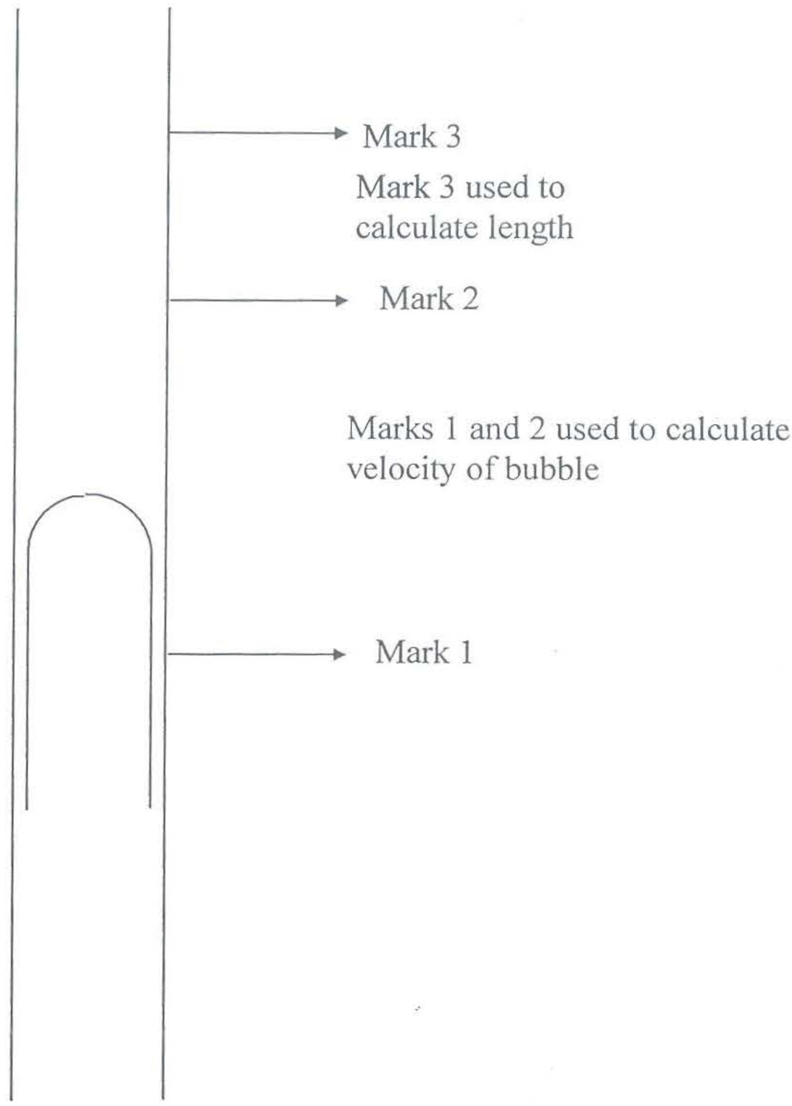

Fig. 4.6. Schematic for bubble length, and velocity calculation

$$Vi = \frac{\Delta d}{t_{1i}} \tag{4.1}$$

where,

V_i = velocity of i^{th} bubble

t_{1i} = time to cross two marks at a distance of 21 cm

$\Delta d = 21$ cm

$$\overline{V} = \frac{\sum_{i=1}^{N} Vi}{N}, \text{N} = 30 \tag{4.2}$$

$$l_i = V_i\, t_{2i} \tag{4.3}$$

where,

l_i = length of the i^{th} bubble

t_{2i} = time for the bubble to cross the third fixed mark

$$\overline{l}\,(\text{by observation}) = \frac{\sum_{i=1}^{N} li}{N},\ N = 30 \tag{4.4}$$

The average length, $\overline{l}$, for a particular set of operation was found to be around 6 cm. This was compared with the value obtained from the data acquisition software. The data obtained was similar to one shown in Fig. 4.2, though the number of rows of zeros was different depending upon the length of bubble. The total time for the bubble to pass through the wire mesh sensor was calculated by taking the time difference between the start of a row with one or two zeroes (depicting the tip of bubble), and end of a row with all zero element beyond which at least one row with all non-zero data was present (depicting the end of a bubble or the start of water phase). In reality, the time spent in the scanning of the 16 nodes should also be taken into account in the calculation of length but since it is only around 356 μs (time for serial transmission is order of millisecond) it is neglected.

$$l_i = \overline{V}\ t_{2i} \tag{4.5}$$

where,

$\overline{V}$ = average velocity of the bubble

t_{2i} = total time between the two sets of rows

l_i = length of the i^{th} bubble

$$\bar{l}(\text{by data acquisition}) = \frac{\sum_{i=1}^{N} li}{N}, \; N = 30 \qquad 4.6$$

The average length for a particular set of data was found to be around 5.53cm. The error between the observed value, and the calculated value was around 0.47 cm. This seems to be a acceptable error, though greater precision is required by getting more number of frames.

4.3 Void Measurement

The next step in the testing of the system was direct measurement of void fraction using a Differential Pressure Transducer (D.P.T.) and comparison with the serial data outputs. A D.P.T. is a device that gives an electrical output depending upon the pressure difference at its 2 input points. The pressure transducer used in the project had a range of 25 inches of water (625 mm of water). It required a D.C. power supply of 24 V. This transducer required the use of a 250 ohm resistor in series with the D.C. supply circuit. The current range of the transducer was 4-20 mA, which translates to the voltage range of 1 – 5 volt for the 250 ohm resistor used. The lower range of the voltage is obtained at zero pressure difference at the two input ends of the D.P.T. The higher range of voltage corresponds to the highest-pressure difference (25 inches or 650 mm of water) at the inputs of the D.P.T. In the present project the longest bubble that could be generated was around 10 cm i.e. around 4 inches. The device was calibrated in the range of 0-160 mm, the range relevant for the project.

A U-tube manometer was used for the calibration of the transducer. The U-tube was filled with water. A schematic for the calibration is shown in Fig. 4.7. When the valve was open and the two screws on the two inputs of the D.P.T. were unscrewed, the water level was same in both the columns of the U-tube. The screws on the inputs are used as valves to drain the fluid in the two tubes connected to inputs. One tube connects an input point of the D.P.T. to one column of the U-tube manometer (the second column was open to atmosphere) while the second tube is connected to another input point of the D.P.T. and is open to atmosphere. The pressure difference between the two inputs of the D.P.T was zero when the water level in the two legs of the manometer was same and thus the output voltage was 1 volt (250 ohm x 4 mA =1 Volt). The zero screw of the D.P.T. was set at this condition. After this, two screws at the inputs of the transducer were closed and air was blown through the valve such that the difference in the level of the two columns of the U-tube reached 160 mm. Then the valve was closed and the span screw was set at this condition. The output was 5 volts as seen on CRO (250 ohm x 20 mA = 5 Volts) Thus the pressure transducer was set to operate in the range of 0-160 mm of water. To get the calibration curve, the main valve (valve through which air was blown) was opened such that the height difference in the two columns of the manometer was reduced by 10 mm from the highest value of 160 mm, and the output voltage was recorded on the CRO. This was repeated until the pressure difference was zero (same level of water in the two columns of the manometer) and output was 1 Volt. The calibration curve i.e. pressure vs. voltage is plotted in Fig. 4.8. Using least square fit, a straight-line function is also shown in the same figure. The transducer was, thus, completely calibrated to suit the purpose of the project. The complete set-up, with D.P.T. connection, is shown again in Fig. 4.9. The D.P.T inputs were connected to the two tappings that were at a distance of 160 mm. The tappings were made symmetrically with respect to the wire mesh. For the D.P.T., a 250 ohm resistor was connected in series to its D.C circuit and output across it was monitored on the CRO. When the cylindrical tube was empty, (only air inside it)

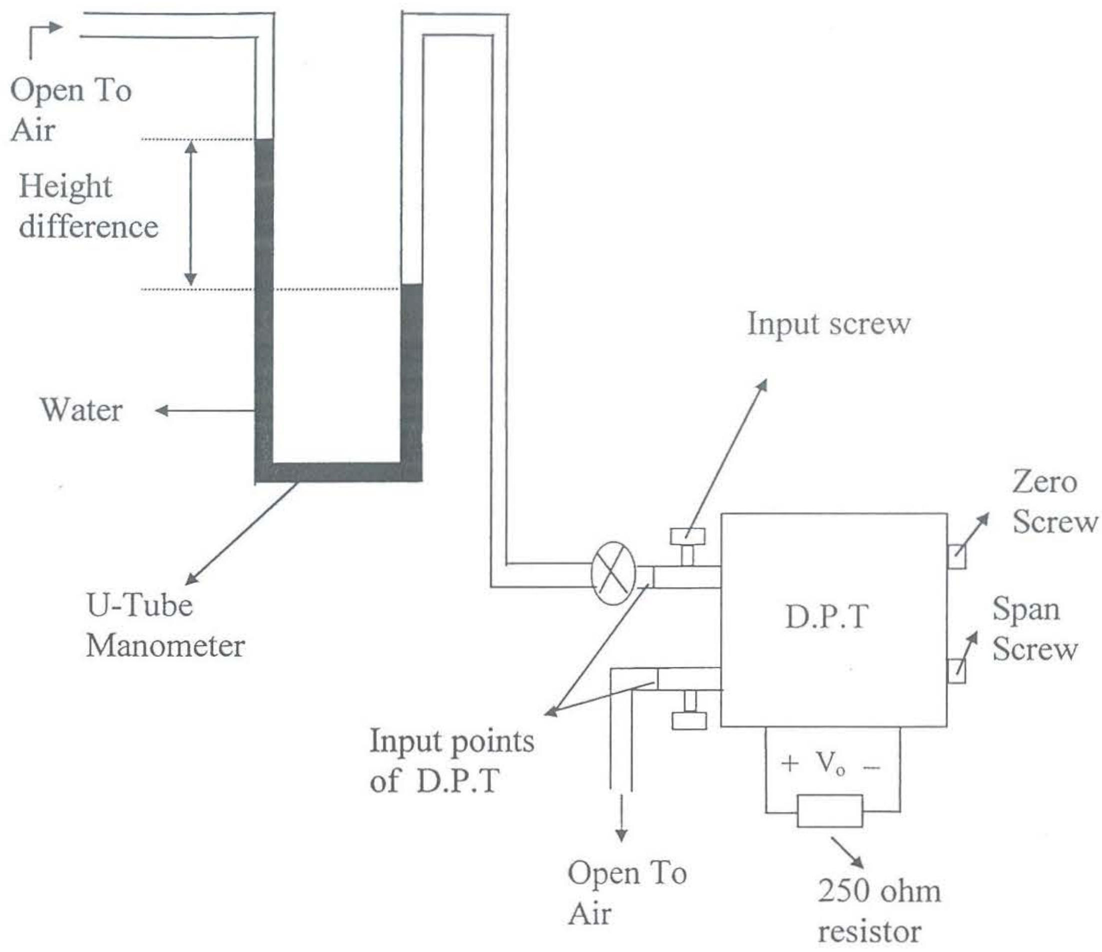

Fig. 4.7. Schematic for calibration of the D.P.T

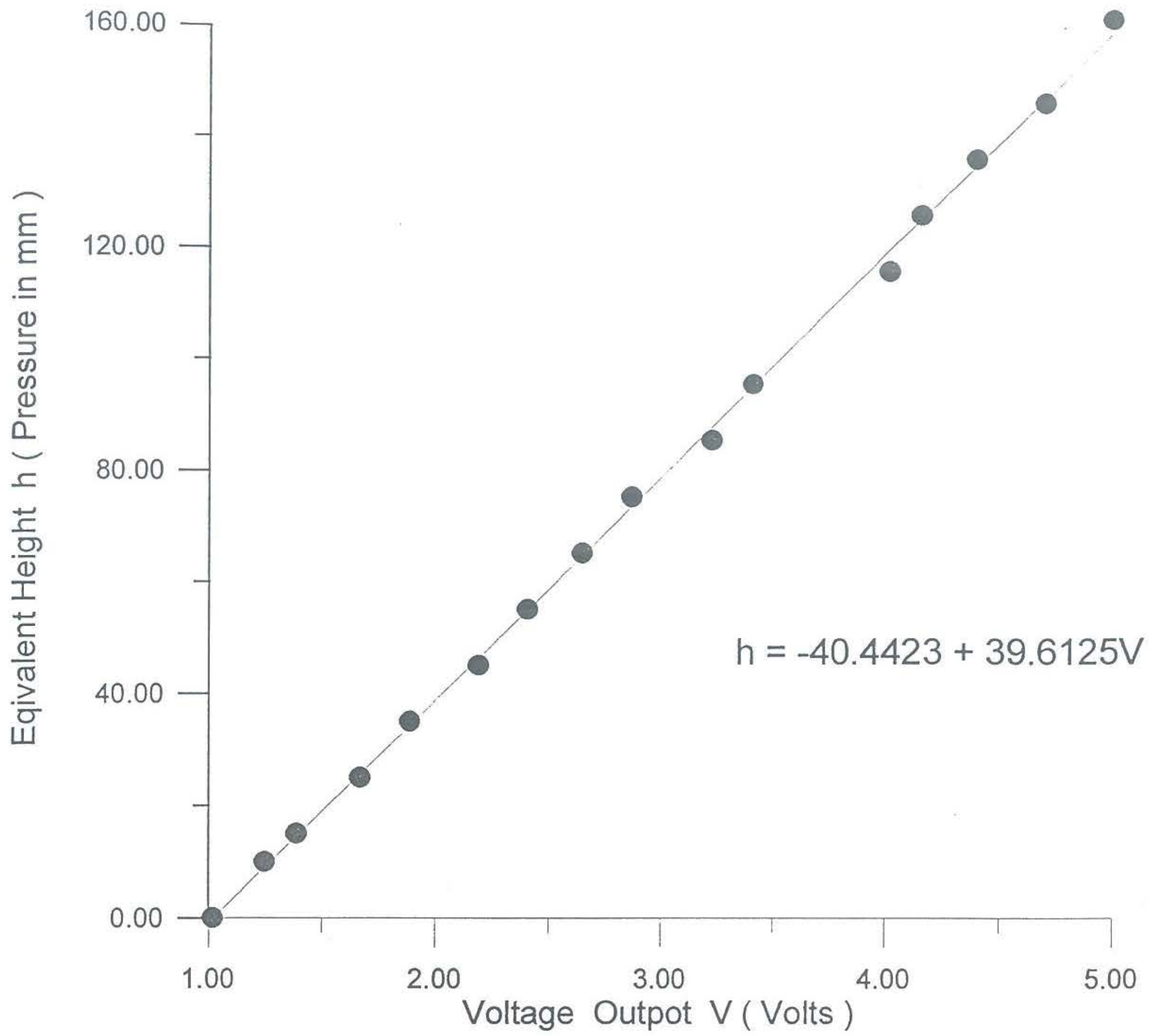

Fig. 4.8. Calibration curve for the D.P.T.

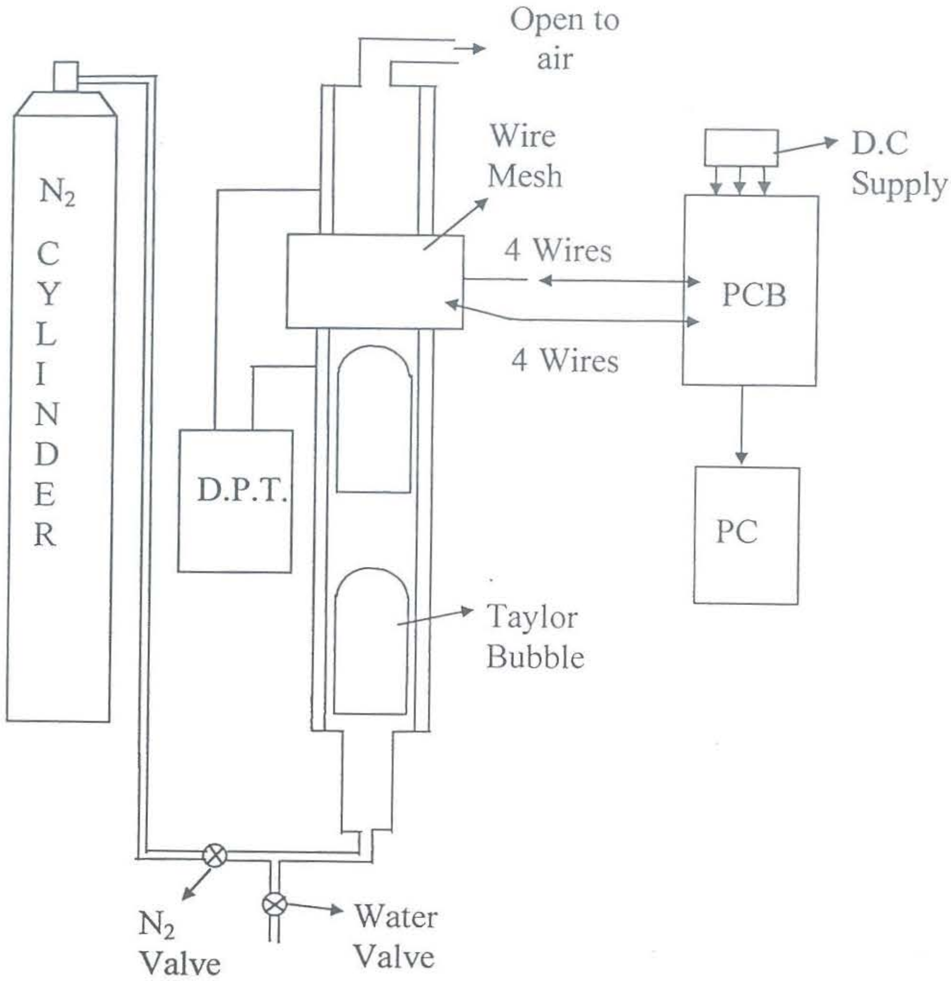

Fig. 4.9. Complete set-up with
D.P.T. connection

the output was 1 Volt since the pressure difference between the two inputs of D.P.T. was $\rho_a gh$ (ρ_a = density of air since nitrogen has density that is very close to air, h = 160 mm). This pressure difference is very small. Water was, then, filled in the tube and the output went up to 5 Volt since the pressure difference was $\rho_w gh$ (ρ_w = density of water = 1000, h = 160 mm). After this, nitrogen at low pressure was passed at the bottom of the tube. The bubbles generated were small, the length being around 2 cm. As these bubbles passed in between the tappings, the output fell down from 5 volt. A typical output, on CRO, is given in Fig. 4.10. The output was taken for a period of around 20 seconds using the storage mode of the CRO. The troughs in the output, shown as V_v, represent the bubbles in between the tappings. These values of V_v were used in the straight-line curve fit between pressure, and voltage to get the pressure drop between the two tappings on the cylindrical tube.

The pressure equivalent in height, neglecting frictional pressure drop, is given by (Appendix B)

$$\Delta P = h = (1 - \alpha)H \qquad 4.7$$

h is calculated from the straight line fit and the voltage output as described earlier.

$$\alpha = 1 - h/H \qquad 4.8$$

To get the value of void fraction by the data acquisition system, serial data was obtained for about 20 second the time for which voltage output from the D.P.T was obtained on the CRO. The data obtained using serial communication system was similar to that shown in Fig. 4.2. Fig. 4.11 shows how this data would appear along the space axis. This is equivalent to saying that in a length L, corresponding volume being V_1, the void fraction is,

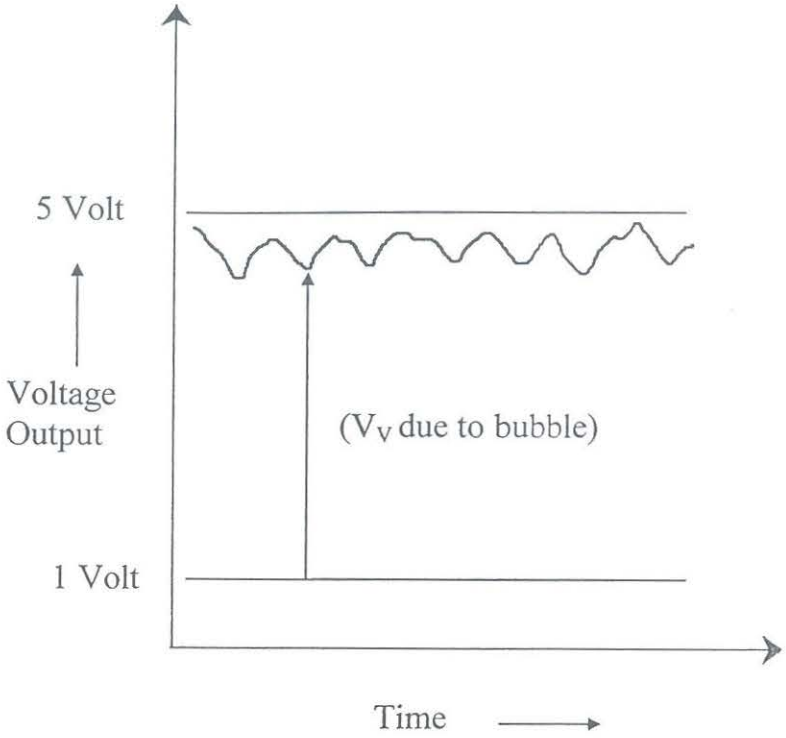

Fig. 4.10. Output voltage on CRO

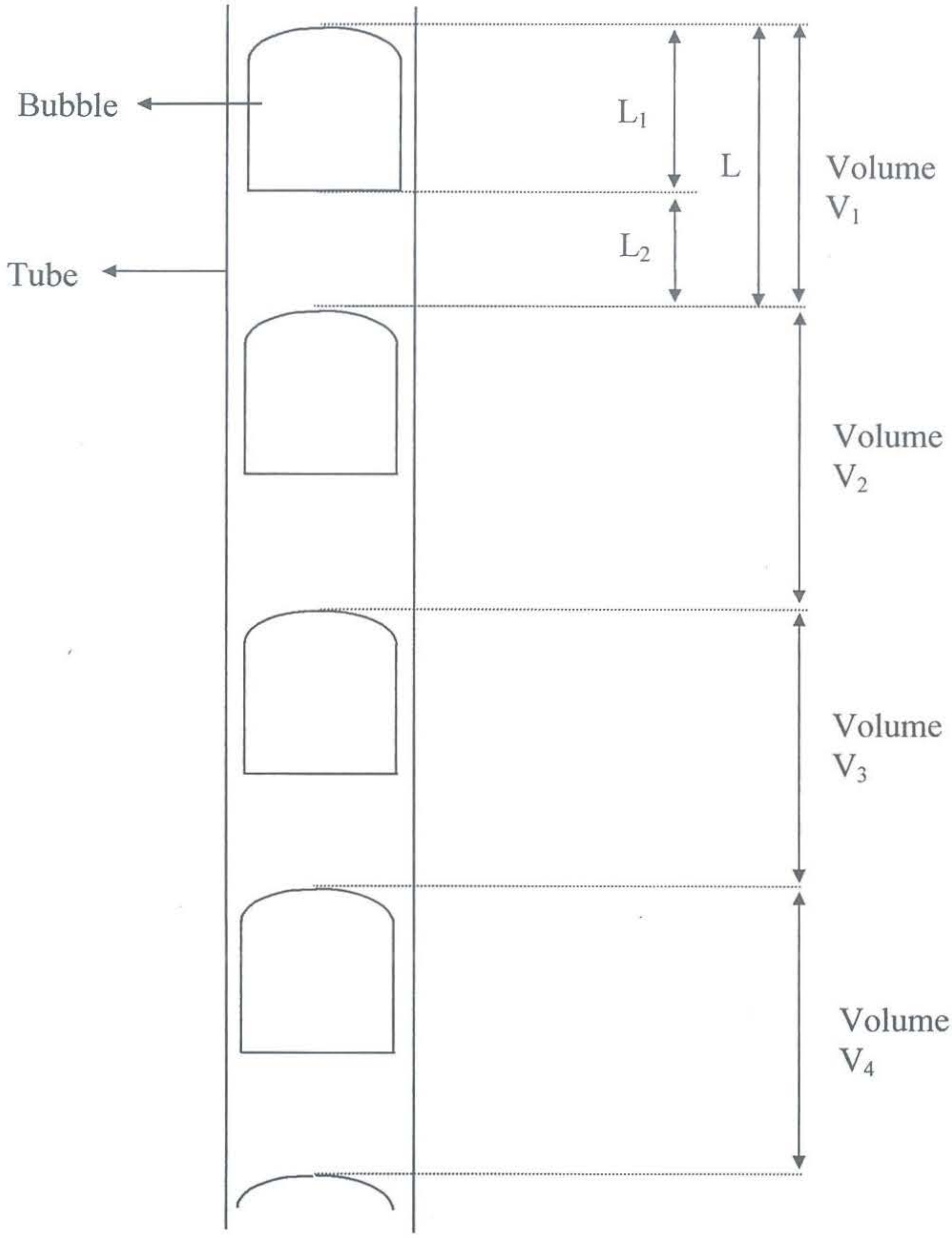

Fig. 4.11. Scheme to calculate void fraction

α = volume of bubble / (volume of bubble + volume of water)

Assuming that bubbles are almost cylindrical,

$$\alpha = L_1 A \; / (L_1 A + L_2 A) = L_1/L \qquad 4.9$$

where, L_1, and L_2 are the lengths of the bubble, and the water section respectively. Length L_1, was calculated by taking the time difference between the data lines showing start and end of a bubble (Fig. 4.2.). Length L_2 was calculated by taking the time difference between data line showing the end of the bubble of length L_1 and start of a bubble in volume V_2. Similar calculations were performed for volumes V_2, V_3.... as shown Fig. 4.11. An average value of the void fraction was obtained using above calculations.

After this experiment, the bubble size was increased gradually and similar calculations for the determination of void fraction using D.P.T and data acquisition system were performed. Six values of void fraction were determined, up to a maximum bubble length of around 8.9 cm. Generation of bubbles greater than 9 cm was very difficult in the present setup. Fig. 4.12 gives a plot of the void fraction obtained by both the methods. The x-axis gives the average value of void fraction obtained by the D.P.T. method and the y–axis gives the average value of void fraction obtained by the data acquisition system. The differences in the values of void factions determined by the two methods occur because of human and system instrument error. These are dealt with in the next chapter and corrective actions sought.

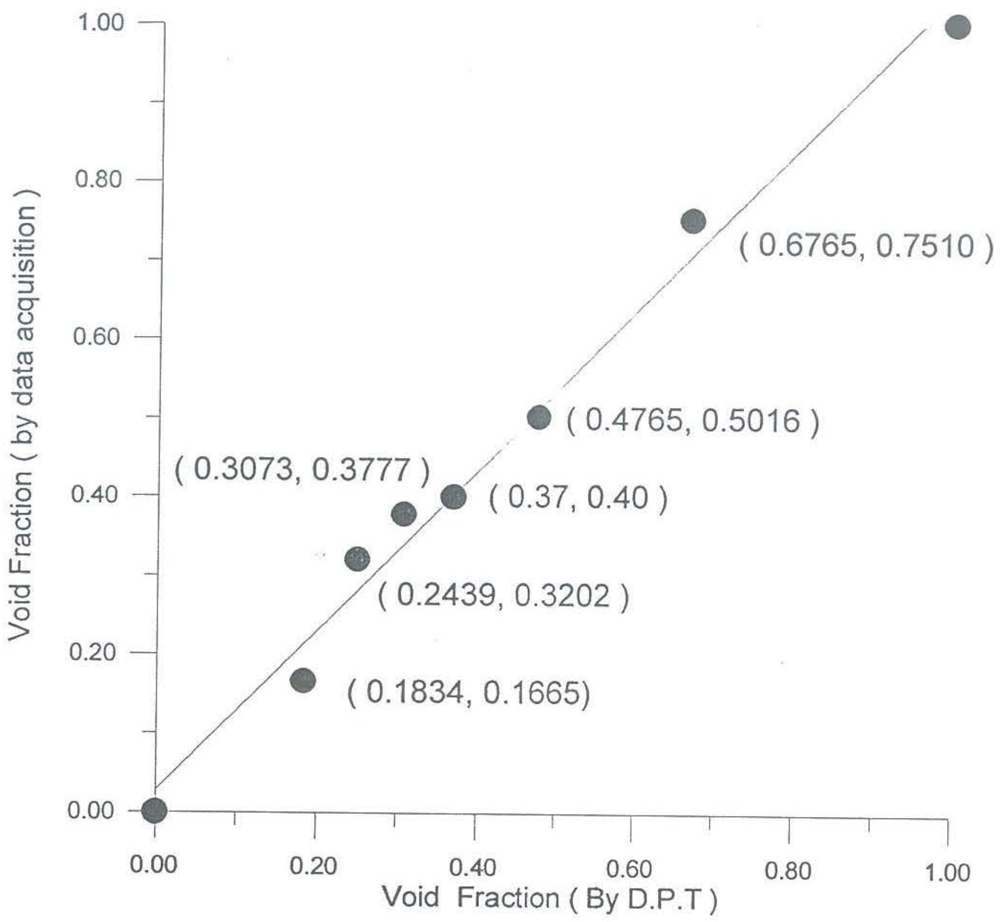

Fig. 4.12. Void fraction by the two methods

Chapter 5

SUMMARY AND CONCLUSION

In the second chapter, literature related to conductance and capacitance probes has been reviewed. A wire mesh type probe reported by Krepper and Prasser [14] was found to be relatively easier in construction, had simple electronic circuit, and the measurement results did not involve any calculation. Based on this work a wire mesh type probe was made for void measurement. A 4 x 4 wire mesh was formed using hypodermic needles. Four wires in this mesh were used as excitation electrodes and the other four wires were used as receiving electrodes. A microcontroller was used to generate input pulses that were fed to low-pass filters and buffer amplifiers. The outputs of the buffers were given to the sending electrodes. The current through the transmitting electrodes was passed to I/V converters and the output of I/V was passed on to ADC's. The outputs of the ADC's were passed to the microcontroller for serial transmission. Before the actual experiment, a two-phase medium was simulated using a resistor network, and the probe electronics was found to be satisfactorily detecting the simulated voids.

Next, the probe system was used to measure void fraction in a two-phase flow set-up. Taylor bubbles were generated in the cylindrical tube using nitrogen cylinder. The wire mesh probe was able to satisfactorily scan a bubble, map the bubble, and give its volumetric distribution in the water column. Using the data obtained for the bubbles void fraction was computed and compared with the void fraction value obtained using D.P.T. The results of the void fraction as calculated by the D.P.T., and the probe matched very closely, the minimum percentage error being 5.26 and the maximum being 31.23.

There were discrepancies in the data, in the first 2-3 rows, for the Taylor bubbles generated at a particular pressure. The reason for this could be that along with the Taylor bubble a number of very small bubbles would pass through the wire mesh and causes a zero in the output of a node that has not been touched by the Taylor bubble. The other reason could be that all the Taylor bubbles do not pass the probe section at the same velocity. There were mainly three sources of error involved in all the measurements. First was the human observational error in estimating the bubble length. Second was the instrument error as in the CRO, and the electronic circuit. The serial transmission rate for the data was 9600 bps. If this could be increased by appropriate component selection, the number of frames obtained for a bubble would be much larger. This would help in mapping a bubble more closely to its actual profile and length. The third reason for the error was that the selection of the 4 x 4 wire mesh generated very less data per frame. The number of physical points to be scanned for the bubble could be increased by putting more number of wires in the two sets of parallel wires. Larger the number of wires larger would be the data per frame. There are two aspects that might restrict the use of a very large number of wires. First is the cost involved in the electronic circuit component, and second is the distortion of void pattern and void fraction due to large number of wires. An optimal value of the number of wires has to be determined to care of these aspects. The concept of cross-sectional scanning has made possible one of the basic objective of void measurement i.e. measurement of void fraction independent of the type of flow. The Taylor bubbles used in the experiment approximately represent annular flow, and slug flow. The problem would come in scanning bubbly flow when the bubble diameter would be smaller than the pitch of the wire mesh, and also in case of misty annular flows. This aspect has to be investigated in depth to make the probe more universally acceptable

APPENDIX A

MP8786: ANALOG-TO-DIGITAL CONVERTER

MP8786 [16] is an 8-bit Analog-to-Digital converter designed for high speed digitizing applications requiring low power. This device uses two-step flash architecture to maintain low power at high conversion rates. A block diagram of the internal architecture is given in Fig. A.1. The input circuitry includes an on-chip S/H. The device operates on a single +5 volt supply. The reference voltage has a of range 0 - 5 V. However, an internally generated reference voltage can be used by connecting the pin V_{RTS} to V_{RT} and pin V_{RBS} to V_{RB}. The internal reference generates 0.6 V at V_{RB} and 2.6 V at V_{RT}. The internally generated reference voltage has been used for the ADC's, used in the electronic circuit for the project. In the conversion process there is a pipeline of four operations: S/H, conversion and latch, encoding and error correction, output latch. All the operations are carried out at each clock. Thus the digital value sampled at a particular clock will become available at the fifth clock. The output enable can be used for reading the latch output onto the digital bus. In case output enable is high, the ADC output lines remain tri-stated.

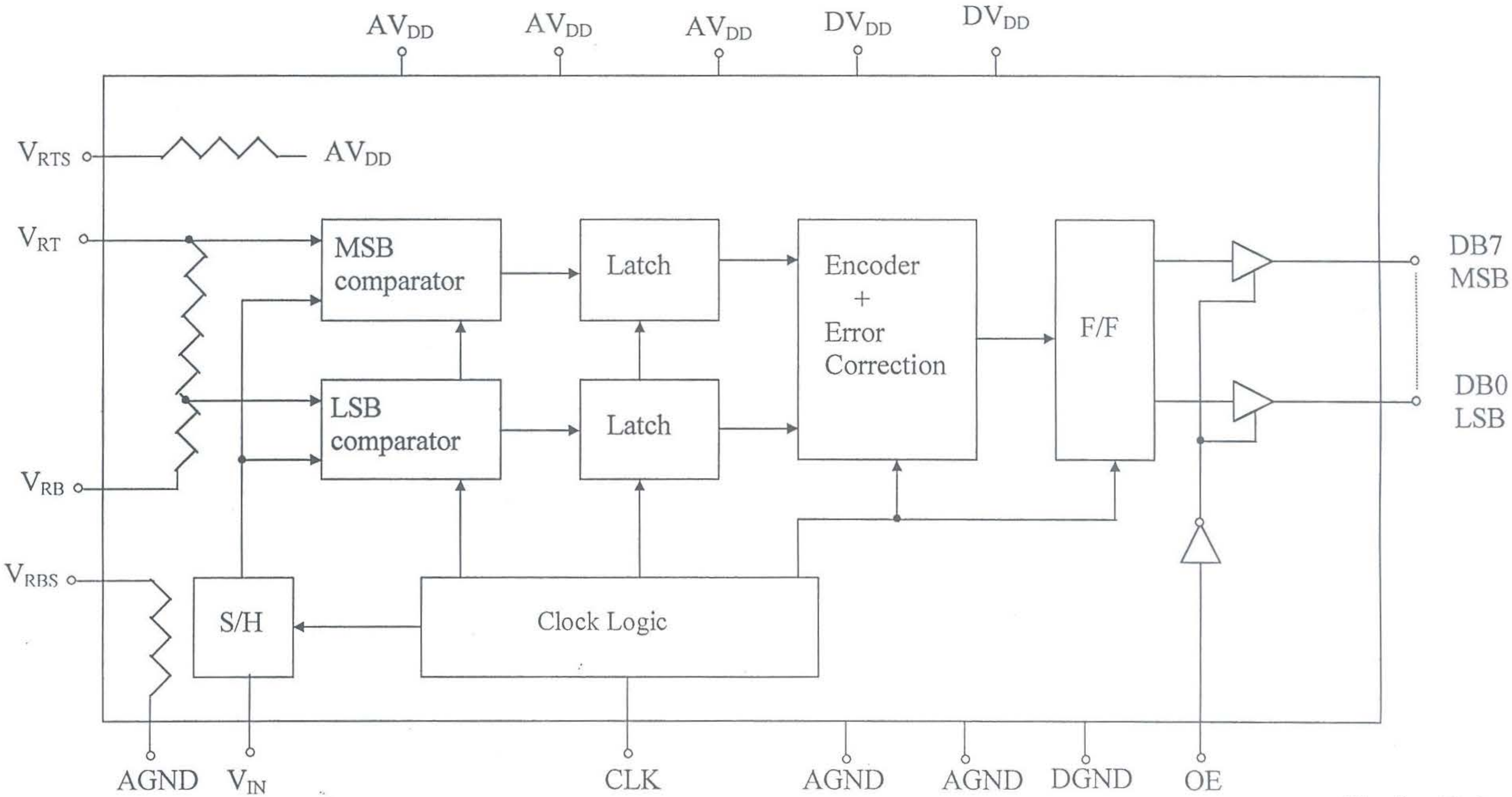

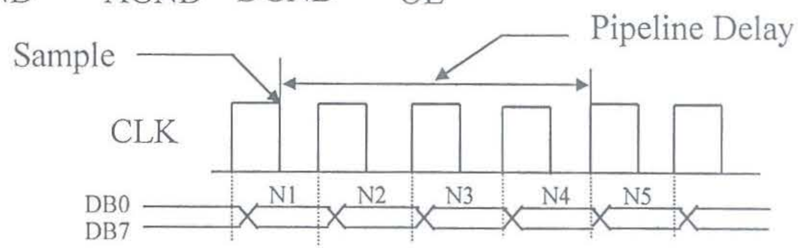

Fig. A.1. Block diagram of the internal Architecture of MP8786 [16]

APPENDIX B

Assume a given volume V, where water and air (in the form of bubbles) is present. Let ρ_w, and ρ_a be the density of water, and air respectively. Let V_1, and V_2 be the respective volumes of water and air. Under an assumption that the water, and bubbles are both moving at the same velocity in the pipe (homogeneous model) or equivalently, everything is static, the density of the mixture, ρ_H, is

$$\rho_H = \text{total mass / total volume} \qquad \text{B.1}$$

$$\text{total mass} = \text{mass of water} + \text{mass of air}$$

$$\text{mass of water} = \rho_w V_1$$

$$\text{mass of air} = \rho_a V_2$$

$$\text{total volume} = V_1 + V_2 = V$$

By the definition of void fraction,

$$V_1 = (1-\alpha) V \qquad \text{B.2}$$

$$V_2 = \alpha V \qquad \text{B.3}$$

$$\rho_H = (\rho_w V_1 + \rho_a V_2) / V$$

$$= \rho_w(1-\alpha) + \rho_a(\alpha) \qquad \text{B.4}$$

In Fig. B.1, a schematic is shown to calculate the pressure difference at the inputs of the D.P.T.

From this figure, neglecting frictional pressure drop,

$$P_2 - P_1 = \rho_H g H$$

$$P_2' = P_2 + \rho_a g H_2'$$

$$P_2' = P_1 + \rho_a g H_1'$$

$$\Delta P = P_2' - P_1' = P_2 - P_1 + \rho_a g(H_2' - H_1') \qquad \text{B.5}$$

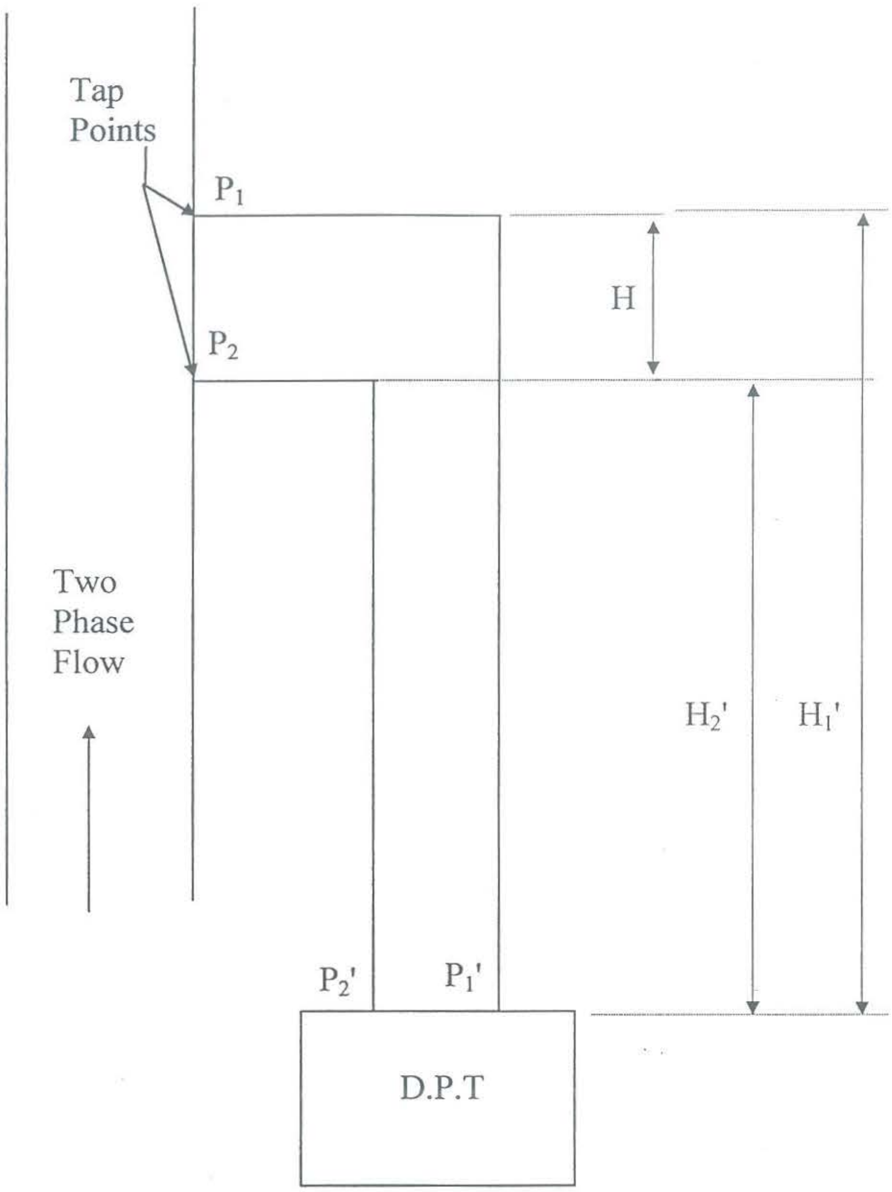

Fig. B.1. Schematic to calculate pressure difference

$$\Delta P = \rho_H gH + \rho_a g\,(-H)$$
$$= [\alpha\rho_a + (1-\alpha)\rho_w - \rho_a]\, gH$$
$$= (1-\alpha)(\rho_w - \rho_a)\, gH \qquad \text{B.6}$$

Since, $\rho_a <<< \rho_w$

$$\Delta P = (1-\alpha)\rho_w gH$$

So, the pressure drop in equivalents of water height (dividing by $\rho_w g$) is,

$$\Delta P = h = (1-\alpha)H \qquad \text{B.7}$$

REFERENCES

[1] Zwahr H., "Das Verhaltenvon Zwei-Phasen –Gemischen in Zentrifuglfeldren", Ph.D. Thesis , Techniche Universitat Hannover, 1976.

[2] Welle R.V.D., "Void Fraction, Bubble Velocity and Bubble Size in Two Phase Flow", *Int.J.Multiphase Flow*, Vol. 11, No.3, 1985, pp. 317-345.

[3] Meftah K. and Ruggles A.E., "Vapor Volume Fraction, Flow Regimes and Vapor Velocity Inference Using Fluid Conductivity Measurements", *Review of Scientific Intruments*, Vol. 69, No.8, Aug. 1998, pp. 2948- 2955.

[4] Andreussi P., Dontrancesco D. and Messia M., "An Impedance Method for the Measurement of Liquid Hold-up in Two-Phase Flow", *Int.J.Multiphase Flow*, Vol. 14, No. 6, 1998, pp. 777-785.

[5] Tsochatzidis N.A., Karappantsias, T.D.,Mostoglou, M.V. and Karabelas A., "A Conductance Probe for Measuring Liquid Fraction in Pipes and Packed Beds" , *Int.J.Multiphase Flow*, Vol. 18, No. 5, 1992, pp. 895-902.

[6] Asali J.C., Hanrtly T.J and Anderussi P., "Interfacial Drag and Film Height for Vertical Annular Flow", *AIChE*, Vol. 31, 1985 , pp. 895-902.

[7] Maxwell J.C., "A Treatise on Electricity and Magnetism", Clarendon Press, Oxford, 1881.

[8] Bruggeman D.A.G., "Calculation of Different Physical Constants of Heterogeneous Substances", *Annln Physica*, Vol. 24, 1935, pp. 626-697.

[9] Merilo M., Dechene R.L. and Chichowlas W.M., "Void Fraction Measurement with a Rotating Electric Field Conductance Gauge", *Journal of Heat Transfer*, Vol. 99, 1977, pp. 330-332.

[10] Abouelwafa M., Sami A. and Kendall E., John M., "The use of capacitor sensors for phase percentage determination in multiphase pipelines", *IEEE*, 1980 , pp. 18-21.

[11] Khalil A., McIntosh G. and Broom R.W., "Experimental measurement of void fraction in cryogenic two phase upward flow", *Cryogenics*, July 1981, pp. 411-414.

[12] Kendoush A.A., and Sarkis Z.A., "A non–intrusive auto transformer technique for the measurement of void fraction", *Experimental Thermal and Fluid Science*, Vol. 13, 1994, pp. 92-97.

[13] Wang J., "A pulse frequency measuring system for the determination of void fraction in cryogenic two-phase flow", *Cryogenics* , Vol. 30, 1990, pp. 308-312.

[14] Krepper E. and Prasser, H.M., "Measurement and CFX- Simulations of a Bubbly Flow in a Vertical Pipe", *Forschungszentrum Rossendorf,* Institute of Safety Research , Germany, 1999.

[15] Linear Databook 1, National Semiconductor , 1988.

[16] EXAR Corporation, "MP8786 CMOS 30 MSPS, 8-bit high speed power Analog to Digital Converter with power down", March , 1998.

[17] Atmel Corporation , 8051 Flash Microcontroller Databook , Dec. 1997.

ACKNOWLEDGEMENT

I would like to thank my guides Prof. Kannan N. Iyer, and Prof. P.C.Pandey for their valuable suggestions, and constant support during the course of preparation of this report. I am also thankful to all my friends and colleagues who had helped me directly or indirectly during the course of my work.

I.I.T., Bombay
8^{th} January, 2001

Mahendra Prasad
(99317301)